KSHV vIL-6 Enhances Inflammatory Responses by Epigenetic Reprogramming

Tomoki Inagaki[1], Kang-Hsin Wang[1], Ashish Kumar[1], Chie Izumiya[1], Hiroki Miura[1], Somayeh Komaki[1], Ryan R. Davis[2], Clifford G. Tepper[3], Harutaka Katano[4], Michiko Shimoda[1], & Yoshihiro Izumiya[1, 3, *]

[1] Department of Dermatology, School of Medicine, the University of California Davis (UC Davis), Sacramento, California USA
[2] Department of Pathology and Laboratory Medicine, School of Medicine, UC Davis, Sacramento, California USA
[3] Department of Biochemistry and Molecular Medicine, School of Medicine, UC Davis, Sacramento, California USA
[4] Department of Pathology, National Institute of Infectious Diseases, Shinjuku, Tokyo, Japan

*Correspondence: Yoshihiro Izumiya DVM, PhD

Address: UCDMC Research III, Room 2200B, 4645 2nd Avenue, Sacramento CA 95817
Email: yizumiya@ucdavis.edu
Phone: 916-734-7253

Abstract

Kaposi sarcoma-associated herpesvirus (KSHV) inflammatory cytokine syndrome (KICS) is a newly described chronic inflammatory disease condition caused by KSHV infection and is characterized by high KSHV viral load and sustained elevations of serum KSHV-encoded IL-6 (vIL-6) and human IL-6 (hIL-6). KICS has significant immortality and possesses greater risks of having other complications, which include malignancies. Although prolonged inflammatory vIL-6 exposure by persistent KSHV infection is expected to have key roles in subsequent disease development, the biological effects of prolonged vIL-6 exposure remain elusive. Using thiol-Linked Alkylation for the Metabolic Sequencing and Cleavage Under Target & Release Using Nuclease analysis, we studied the effect of prolonged vIL-6 exposure in chromatin landscape and resulting cytokine production. The studies showed that prolonged vIL-6 exposure increased Bromodomain containing 4 (BRD4) and histone H3 lysine 27 acetylation co-occupancies on chromatin, and the recruitment sites were frequently co-localized with poised RNAPII with associated enzymes. Increased BRD4 recruitment on promoters was associated with increased and prolonged NF-κB p65 binding after the lipopolysaccharide stimulation. The p65 binding resulted in quicker and sustained transcription bursts from the promoters; this mechanism increased total amounts of hIL-6 and IL-10 in tissue culture. Pretreatment with the BRD4

inhibitor, OTX015, eliminated the enhanced inflammatory cytokine production. These findings suggest that persistent vIL-6 exposure may establish a chromatin landscape favorable for the reactivation of inflammatory responses in monocytes. This epigenetic memory may explain the greater risk of chronic inflammatory disease development in KSHV-infected individuals.

Author summary

Combined and continuous cytokine stimulation triggers transcription reprogramming and is often used for specific tissue development. Continuous vIL-6 exposure occurs in KSHV-infected patients and leads to inflammatory cytokine storm with high mortality. However, possible epigenetic reprogramming by the vIL-6 and its association with pathogenesis remain unclear. Here we demonstrate the establishment of a new chromatin landscape mediated by BRD4 through prolonged vIL-6 exposure which contributes to more robust and rapid transcription and increased cytokines production. Inhibition of BRD4 suppressed this inflammatory response. Our results indicate that targeting the epigenetic effect of viral cytokines may lead to novel therapies for KSHV-induced inflammatory cytokine storms.

57 **Introduction**

58 Controlled inflammatory response enhances host immunity against external insults,
59 whereas uncontrolled inflammatory responses resulting from excessive cytokine
60 production leads to disruption of such balance. In particular, monocytes and
61 macrophages play major roles in controlling pro-inflammatory cytokines expression and
62 their tightly controlled activation is critical for regulating systemic inflammation in our body.
63 Previous reports have shown that continuous inflammatory stimulation enhances [1, 2] or
64 sometimes impairs [3, 4] responses to subsequent stimulus. In either case, continuous
65 inflammatory stimulation appears to alter the cellular phenotype and affect inflammatory
66 cytokine production.

67 Kaposi's sarcoma-associated herpesvirus (KSHV) was first identified in Kaposi's
68 sarcoma (KS) lesions in 1994 [5]. KSHV is also associated with lymphoproliferative
69 diseases, primary effusion lymphoma (PEL) and multicentric Castleman's disease (MCD)
70 [6, 7]. Recent studies showed that KSHV infection also causes severe systemic
71 inflammation, which is categorized as Kaposi's sarcoma-associated herpesvirus
72 inflammatory cytokine syndrome (KICS) [8]. KICS is characterized by increased viral
73 loads and inflammatory cytokines such as human IL-6 (hIL-6), IL-10, and KSHV-encoded

74 interleukin-6 homolog, viral IL-6 (vIL-6). Individuals with KICS are known to have a higher
75 risk of developing KSHV-associated cancers and other malignancies [8].

76 The vIL-6, encoded by KSHV ORF-K2, is expressed during the lytic replication
77 phase, and single cell transcriptomics studies also suggested that vIL-6 may be
78 expressed during latency in selected cell populations [9]. Similar to hIL-6, vIL-6 is known
79 to enhance cell proliferation, endothelial cell migration, and angiogenesis by upregulating
80 vascular endothelial growth factor (VEGF) [10] and downregulates the caveolin 1
81 expression [11-13]. Moreover, vIL-6 transduction also leads to cell transformation in the
82 3T3 cells model and induces tumors in xenograft mice [10]. Increased metastasis is also
83 seen in a murine xenograft model with transgenic vIL-6 mice [14]. The vIL-6 activates
84 downstream signaling pathways by binding to the cellular hIL-6 receptor, gp130.
85 Dimerization of gp130 induced by hIL-6 binding activates Janus tyrosine kinases and
86 phosphorylates the SH2-containing cytoplasmic protein STAT3 (signal transducer and
87 activator of transcription 3). The phosphorylated STAT3 forms a dimer and translocates
88 to the nucleus to activate the downstream genes that play essential roles in inducing the
89 inflammatory response, cell survival, and immune responses [15-17].

90 Synergistic interactions between another inflammatory-associated transcription
91 factor, nuclear factor-kappa B (NF-κB) and STAT3 are known to induce the

92 hyperactivation of NF-κB followed by the production of various inflammatory cytokines
93 including TNFα and hIL-6. Because hIL-6 expression is regulated by NF-κB pathway
94 activation, simultaneous activation of NF-κB and STAT3 triggers a positive feedback loop
95 of NF-κB activation in the hIL-6/STAT3 axis. This positive feedback loop is called the IL-
96 6 amplifier (IL-6 Amp) and is a key element in inflammatory disease development [18]. In
97 the IL-6 Amp disease model, obesity, injury, and infection trigger chronic inflammation
98 and/or a systemic cytokine storm, which is enhanced by interactions between local non-
99 immune cells and infiltrating immune cells [18]. A prominent example of IL-6 Amp is also
100 seen in Coronavirus disease 2019 (COVID-19), which is triggered by severe acute
101 respiratory syndrome coronavirus 2 (SARS-CoV2) infection [18]. Consistent with the
102 significance of hIL-6 in disease development, a humanized monoclonal antibody against
103 the hIL-6 receptor, tocilizumab, has proven successful for treating Castleman's disease
104 as well as COVID-19 [19, 20]. In the case of KSHV-associated diseases, the IL-6 Amp
105 may be triggered by KSHV infection and is likely to be associated with vIL-6 expression
106 from KSHV-infected cells. However, how persistent exposure of vIL-6 alters cellular
107 responses and enhances inflammation cytokine production remain elusive.

108 The bromodomain and extraterminal domain (BET) family proteins such as
109 bromodomain containing 4 (BRD4) are transcription regulators, which localize to cellular

110 enhancer and promoter loci and control the transcription of a wide range of
111 proinflammatory genes. BRD4 regulates transcription by recognizing acetylated histone
112 tail and interacts with transcription factors such as NF-κB p65 and transcription elongation
113 complex [21]. This mechanism facilitates the phosphorylation of RNAPII and therefore
114 promotes transcription initiation and elongation. In the context of proinflammatory gene
115 activation, interaction with NF-κB p65 is especially important, because p65 itself is
116 acetylated at K218, K221, and K310, and the acetylated K310 is recognized by the BRD4
117 bromodomain to form an active transcription complex [22]. In addition to the specific
118 protein-protein interactions, BRD4 also forms nuclear puncta on super-enhancer genomic
119 regions that exhibit properties of liquid-like condensates [23]. The intrinsically disordered
120 regions (IDRs) of BRD4 are responsible for phase-separated condensates formation with
121 other coactivators on the chromatin loci for transcription elongation [23], which suggests
122 that enrichment of BRD4 at specific enhancers or promoters are key for selection of genes
123 for activation.

124 Here we demonstrate that a biological effect of prolonged vIL-6 exposures alters
125 the chromatin landscape changes which provides a putative mechanism of
126 overexpression of inflammatory cytokines in vIL-6 pre-exposed cells. We show that an
127 increased amount of BRD4 on chromatin by the prolonged vIL-6 exposure is responsible

128 for transcription deregulation, and repetitive activation of STAT3 appeared to be
129 responsible for the change. BRD4 accumulation prolongs transcription activity at targeted
130 sites with a secondary stimulus by prolonging transcription factor binding and duration of
131 transcriptions. This epigenetic memory may explain the greater risk of chronic
132 inflammatory disease development in KSHV-infected individuals.
133

Results

Biological effects of prolonged vIL-6 exposure on gene transcription and phenotypes

In contrast to temporally regulated hIL-6 expression during wound healing, persistent KSHV infection leads to continuous vIL-6 production from infected cells. Especially, vIL-6 is detected in the serum of KICS patients and the hematopoietic cells in Castleman's disease patients with a high KSHV viral load [24]. To study the biological consequences of vIL-6 exposure, we first purified recombinant vIL-6 protein from recombinant baculovirus-infected cells and confirmed its biological activity by STAT1 and STAT3 activation [25]. In the study, we showed that longevity and strong phenotypic changes in primary monocytes were induced by vIL-6 exposure for at least 9 days [25]. Here, we prepared for a cell culture model with THP-1 cells which were exposed to vIL-6 continuously for two weeks (we refer to vIL-6/THP-1 hereafter) **(Fig. 1A)**. THP-1 cells, a representative monocyte cell line, was employed because monocytes play a major role in inflammatory responses [26]. Using this cell culture model, we compared the overall transcriptional profiles between vIL-6/THP-1 and parental THP-1 cells followed by secondary stimulation with selected cytokines. We used vIL-6 (100ng/ml) and hIL-6

151 (100ng/ml), which can activate common downstream signaling pathways, and TGF-
152 β (100ng/ml), which has a non-overlapping pathway, as a secondary stimulation.
153 To evaluate the newly synthesized RNAs by cytokines stimulation, thiol (SH)-
154 Linked Alkylation for the Metabolic sequencing of RNA (SLAM-seq) was employed [27].
155 vIL-6/THP-1 and parental THP-1 cells were unstimulated or stimulated by vIL-6, hIL-6
156 or TGF-β for 30 minutes, followed by incubation with 4-thiouracil (4sU) for 60 minutes to
157 label transcribing RNAs during the incubation periods. In this experimental setting,
158 sequence reads with mutations T>C identify the only nascent synthesized mRNA
159 because 4sU incorporation with chemical alkylation forces incorporation of G instead of
160 A at 4sU positions during the reverse transcription step [27]. Isolated sequence reads
161 with T>C mutation(s) were then compared among control (non-stimulation), vIL-6, hIL-6,
162 and TGF-β **(Fig.1A)**. As shown in **Fig. 1B**, principal component analysis (PCA)
163 demonstrated clearly distinct cellular responses in vIL-6/THP-1 and also among stimuli.
164 In response to vIL-6 stimulation, we observed that the number of upregulated genes (log2
165 fold change >1, adjusted *p*-value < 0.01) in vIL-6/THP-1 was about twice as many as
166 those with parental THP-1 cells (**Fig. 1C, left**). Similar responses were also seen with
167 hIL-6 as a secondary stimulation (**SFig. 1A**). The vIL-6 and hIL-6 secondary stimulation
168 showed very similar transcriptional profiles (**SFig. 1B**) and downstream pathways (**SFig.**

169 **1C**), suggesting that vIL-6 is clearly a functional homolog of hIL-6. On the other hand, the
170 number of upregulated genes with the TGF-β was slightly decreased in vIL-6/THP-1
171 compared to parental THP-1 cells (**Fig. 1C, right**). In addition, the degree of up-regulated
172 gene expression by vIL-6 or hIL-6 was also increased to a greater extent in vIL-6/THP1
173 cells compared to parental THP-1 cells (**Fig. 1D, SFig. 1D**), while there was no significant
174 differences with TGF-β (**Fig. 1D**). The results suggested that the enhanced transcription
175 response is a pathway dependent. Gene Ontology (GO) analysis indicated that genes
176 related to immune response, Th2 cell differentiation and inflammatory response were
177 commonly enriched by secondary vIL-6 stimulation in parental and vIL-6/THP-1 cells (**Fig.
178 1E: light green**), while cell cycle and cell division pathway were additionally activated in
179 vIL-6/THP-1 cells (**Fig. 1E: green**). Consistent with the GO analysis, cell proliferation was
180 increased in vIL-6/THP-1 cells measured by MTT assay (**SFig. 1E**). Despite an increased
181 number of responding genes with the prolonged vIL-6 exposure, the degree of STAT3
182 activation and gp130 expression (cell surface receptor for vIL-6) was not changed (**SFig.
183 1F, G**).

184 Since KICS patients are characterized not only by increased high vIL-6 or hIL-6
185 but also by increased viral loads, we also examined the effect in KSHV genes expression
186 during de novo infection in vIL-6/THP-1 cells [8]. For this, we infected THP-1 and vIL-

187 6/THP-1 cells with r219.KSHV and performed total RNA-sequencing (RNA-seq). As
188 shown in **Fig. 1F**, overall KSHV gene expression was higher in vIL-6/THP-1 cells
189 compared to parental THP-1 cells. Moreover, vIL-6 and PAN-RNA expression were
190 significantly higher in vIL-6/THP-1 compared to parental THP-1 cells (**Fig. 1G**).
191 Surprisingly, vIL-6 was transcribed as much as PAN RNA in THP-1 cells (**Fig. 1G**). These
192 results suggested that prolonged vIL-6 exposure enhances transcriptional response to
193 secondary vIL-6 and hIL-6 stimulation, and further assists KSHV genes transcription in
194 vIL-6 pre-treated THP-1 cells.
195

196 **Prolonged vIL-6 stimulation increased BRD4 occupancies on chromatin**

197 The studies above demonstrated that prolonged vIL-6 exposure increased the number of
198 responding genes followed by vIL-6 or similar (hIL-6) stimuli without altering the amounts
199 of signal-dependent transcription factor (STAT3). These results led us to examine
200 chromatin modification changes induced by prolonged vIL-6 exposure. For this, we first
201 used CHIP-Atlas, a data mining tool for predicting proteins bound to promoters of
202 upregulated genes based on a comprehensive epigenetic database to narrow down
203 possible epigenetic factors. As shown in **Fig. 2A**, STAT1 and STAT3 were commonly
204 extracted as putative responsible transcriptional factors with vIL-6 stimuli both in parental

205 THP-1 and vIL-6/THP-1 cells, demonstrating the validity of this enrichment analysis.
206 Interestingly, transcription coactivators and several transcription factors such as Cyclin
207 dependent kinase 8 (CDK8), Mediator complex subunit 12 (MED12) and Bromodomain-
208 containing protein 4 (BRD4), are likely to be enriched only in the genomic loci in vIL-
209 6/THP-1 cells (**Fig 2A**). BRD4 is a member of the BET (bromodomain and extra terminal
210 domain) family and an important coactivator that binds to H3K27Ac to mediate
211 transcription regulation together with CDK8, MED12 and RNA polymerase II (RNAPII)
212 [28]. Because BRD4 was identified as the most enriched transcription regulator with
213 prolonged vIL-6 exposure (**Fig. 2B**), we next performed Cleavage Under Targets &
214 Release Using Nuclease (CUT&RUN) for BRD4 and RNAPII. In addition, two active
215 histone modification marks (H3K27Ac, H3K4me3) and CTCF were examined to reveal
216 changes in chromatin landscape [29]. Parental THP-1 cells and vIL-6/THP-1 cells were
217 compared in duplicate samples for statistical analyses. Consistent with the CHIP-Atlas
218 results, BRD4 was more enriched in the transcription start sites of up-regulated genes in
219 vIL-6/THP-1 cells (**SFig. 2A**). We also found that BRD4 and H3K27Ac peaks were
220 increased across the genome in vIL-6/THP-1 cells while RNAPII and H3K4me3 were
221 unchanged (**Fig. 2C**). Immunoblotting showed that the total amount of BRD4 modification
222 was not affected with prolonged vIL-6 exposure, as well as H3K27Ac or H3K4me3,

223 demonstrating that increased BRD4 in vIL-6/THP-1 was from the non-chromatin bound
224 fraction **(SFig. 2B)**. HOMER motif analysis for newly accumulated BRD4 genomic regions
225 identified several key monocyte transcription factors such as E74, ETS Transcription
226 Factor 4, and PU.1 (**SFig. 2C**). PU.1 was also identified as a transcriptional factor likely
227 to be involved in gene activation seen in prolonged vIL-6 exposure by SLAM-seq **(Fig.**
228 **2A)**.

229 We next examined the position and association of the newly accumulated BRD4
230 with H3K27Ac to reveal the changes of active genomic hubs. The CUT&RUN studies
231 identified 31,929 new H3K27Ac regions, while 21,124 regions found in parental cells were
232 no longer modified by H3K27Ac in vIL-6/THP-1 cells **(Fig. 2D).** As shown in **Fig. 2E**,
233 BRD4 was enriched more significantly and sharply at the centers of H3K27Ac peaks in
234 vIL-6/THP-1 cells. The genomic regions, where BRD4 and H3K27Ac peaks overlap, were
235 also increased from 18,886 to 27,509 by prolonged vIL-6 exposure (**SFig. 2D**), suggesting
236 that newly accumulated BRD4 was recruited in newly established H3K27Ac loci in vIL-
237 6/THP-1 cells (**Fig. 2F**). RNAPII and H3K4me3 were also enriched in the genomic regions,
238 where BRD4 and H3K27Ac peaks overlapped (**SFig. 2E**). Closer examination of these
239 enriched sites demonstrated that while the overall number of BRD4/H3K27Ac overlapped
240 peaks around TSS was increased (**Fig. 2G**), the relative abundance of the peaks at the

241 promoter region decreased from 15.4% to 13.5 % in vIL-6/THP-1 cells (**Fig. 2H**). These
242 results may suggest that a larger fraction of newly generated active hubs is located at
243 intragenic regions, perhaps at newly activated enhancers. The CUT&RUN results with
244 the CTCF antibody also suggested that prolonged vIL-6 stimulation increased overall co-
245 occupancies between CTCF and BRD4 across the genome (**Fig. 2I**), suggesting the
246 establishment of activated chromatin hubs in vIL-6/THP-1 cells. The new BRD4 and
247 H3K27Ac peaks were co-localized to promoter regions of genes associated with cellular
248 response to DNA damage stimulus and cell division, such as cyclin E1, which is consistent
249 with the results from the SLAM-seq analysis **(SFig. 2F, G)**.
250

251 **Enhanced response to LPS via prolonged vIL-6 stimulation**

252 Synergistic interactions between NF-κB and STAT3 induce the hyperactivation of NF-κB
253 followed by the production of various inflammatory cytokines such as hIL-6 [18]. KSHV-
254 infected cells are known to have elevated NF-κB activation and STAT pathways are
255 constitutively activated in primary effusion lymphomas [30, 31]. Accordingly, we examined
256 if repetitive STAT activation by vIL-6 exposure alters NF-κB mediated cell responses in
257 *cis.* To study this, we stimulated vIL-6/THP-1 cells with LPS, a strong inducer of NF-κB
258 pathway activation, and examined the cellular response. We first confirmed that 100 ng/ml

259 of LPS stimuli for 6 hours is sufficient for detecting hIL-6 production by ELISA assay **(SFig.**
260 **3A)**, and selected this as a time point to collect samples in order to minimize the
261 secondary effects from the newly produced cytokines with LPS stimuli. We measured a
262 series of downstream inflammatory cytokines produced with Olink, a multiplex proximity
263 extension assay (PEA) [32]. The results showed that LPS upregulated the expression of
264 21/41 inflammatory cytokines (log2 fold change >1) in parental THP-1 cells (**Fig. 3A**).
265 Among them, the expression of 15 cytokines, such as hIL-6, IL-10, IL-1β, and CCL8, was
266 enhanced in vIL-6/THP-1 cells compared to parental THP-1 cells (**Fig. 3A, B**). IFNα
267 stimulation also induced more cytokines in vIL-6/THP-1 cells similarly to that of LPS
268 stimulation (**SFig. 3B, C**), suggesting that prolonged vIL-6 exposure to monocytes
269 sensitized cells to secondary stimuli, reinforcing the notion that enhanced activation is
270 due to the formation of active chromatin complexes at local chromatin.

271 The transcription profile in response to LPS was also accompanied by SLAMseq
272 analysis. LPS (100ng/ml) and 4sU were added to parental THP-1 cells or vIL-6/THP-1
273 cells at the same time and incubated for 6 hours to label nascent transcribed RNAs. PCA
274 demonstrated that LPS strongly changed the gene transcription profile, and the variance
275 between THP-1 and vIL-6/THP-1 cells was further increased by LPS stimulation (**Fig. 3C**).
276 As expected, the inflammatory response was identified as the most enriched pathway in

277 commonly up-regulated genes (N = 1626) (**Fig. 3D**). Next, we investigated whether the
278 increased BRD4 and H3K27Ac occupancies in vIL-6/THP-1 cells contributed to the
279 increased inflammatory gene transcription by LPS stimulation. Commonly up-regulated
280 genes were extracted and the peak scores of the BRD4 and H3K27Ac overlapping
281 regions in THP-1 and vIL-6/THP-1 cells were compared (**Fig. 3E**). As shown in **Fig. 3F**,
282 co-occupancy of BRD4 and H3K27Ac was indeed associated with increased transcription
283 activation with LPS. The increased responses to LPS stimuli were also associated with
284 an increased BRD4 and H3K27Ac co-occupancy compared to genes whose expression
285 was not changed (**Fig. 3G**). These results suggested that prolonged vIL-6 exposure
286 enhances the inflammatory response via increased acetylation of H3K27 at BRD4
287 recruited sites.
288

289 **BRD4 is responsible for prolonging the hIL-6 transcription burst with LPS**

290 Because BRD4 was enriched in the promoter regions of hIL-6, hIL-10 and IL-1β with the
291 prolonged vIL-6 exposure **(SFig. 4A)** and are associated with increased production of
292 cytokines in culture media **(Fig. 3A)**, we next studied how BRD4 recruitment contributes
293 to increasing transcripts. We speculated that increased occupancies of BRD4, which
294 contains an intrinsically disordered domain to form liquid-liquid phase separation (LLPS)

295 [33], may increase the recruitment and duration of p65 binding at promoter regions. This
296 mechanism may extend the duration or robustness of transcription after stimulation.
297 Accordingly, we examined the recruitment of p65 after LPS stimuli in vIL6/THP-1 cells
298 and compare it with parental THP-1 cells. The proximity ligation assay showed that the
299 association between BRD4 and p65 was increased after LPS stimulation in vIL6/THP-1
300 cells (**Fig. 4A**), while the total p65 amount in the nucleus after LPS stimulation was not
301 significantly changed in vIL-6/THP-1 cells (**Fig. 4B**). Chip-qPCR also showed increased
302 p65 recruitment on the hIL-6, IL10, and IL-1β promoters by LPS stimuli in vIL6/THP-cells
303 (**Fig. 4C**). Transcription frequencies were also determined by qRT-PCR analysis of
304 nascent RNA **(SFig. 4B)**. As shown in **Fig. 4D**, hIL-6, IL-10 and IL-1β transcripts were
305 produced more rapidly (hIL-6 and IL-10) and/or continuously (IL-1β) in vIL-6/THP-1 cells
306 after stimulation. Importantly, BRD4 occupancies are responsible for the increased
307 transcription, because OTX-015, a BRD4 inhibitor, drastically suppressed the
308 transcription in both parental THP-1 and vIL-6/THP-1 cells, and the effect was more
309 pronounced in vIL-6/THP-1 cells (**Fig. 4E**). Taken together, prolonged vIL-6 exposure
310 changed the chromatin landscape to be favorable to the response of inflammatory
311 secondary stimuli, and establishment of active chromatin hubs with BRD4 recruitment is
312 critical for this response (**Fig. 5**).

313 **Discussion**

314 In this study, we applied SLAM-seq for most of the RNA-seq experiments to increase the
315 resolution to identify direct target genes (**Fig. 1, 3C**). A short window after the respective
316 stimuli was utilized to examine robustness and differences made in direct target gene
317 expression with prolonged vIL-6 stimuli. By measuring nascent RNA that was labelled
318 shortly after stimulation, we also avoid indirect, or secondary activation. The study clearly
319 demonstrated that direct target genes are significantly overlapped with that of hIL-6
320 (**Fig.1B**). This also suggests that these two signaling ligands are interchangeable, making
321 it easier to have a continuously stimulated IL-6 signaling pathway in KSHV infected
322 individuals.

323 Cytokines that activate STAT3 (e.g. hIL-6) and NF-κB (e.g. TNF- α)
324 synergistically increase the production of various inflammatory cytokines, called IL6-Amp.
325 Since vIL-6 has the same biological activity as hIL-6 **(Fig.1B, SFig. 1B, C),** it is reasonable
326 to speculate that vIL-6 bypasses hIL-6 expression to trigger the IL6-Amp in vivo. The vIL-
327 6 can bind to gp130 alone and does not require the high affinity IL-6 receptor [34, 35].
328 This is in clear contrast to hIL-6, which must bind to its high affinity receptor before a
329 signaling complex can be formed with its signal transducer, gp130 [36, 37]. Importantly,
330 the gp130 is widely expressed in human tissues, and the notion that vIL-6 activates

331 downstream JAK/STAT pathway without requiring binding to the classical gp80 receptor
332 [38-41] suggests that vIL-6 would initiate signaling in a wider variety of cell types [40, 42].
333 In addition, previous studies by Dr. Nicholas's group further demonstrated that vIL-6 can
334 function though intracellularly via activation of gp130 at the endoplasmic reticulum in
335 infected cells [43, 44]. The study suggested that vIL-6 may support the growth and
336 survival of KSHV-infected cells in an autocrine manner and such unique signaling
337 activities contribute to the maintenance of latently infected cells without alarming
338 bystander cells. Our recent study with primary monocyte infection as well as this study
339 agreed very well with the observation, in which prolonged vIL-6 stimuli shifted the cell
340 transcription program towards cell growth and anti-apoptotic signaling (**Fig. 1E, SFig. 1E**).
341 More importantly, similar phenotypes were also seen in wild-type KSHV primary infection
342 but not infection with vIL-6 stop virus [25].

343 Prolonged vIL-6 stimuli similarly increased the number of responding genes to
344 secondary vIL-6 and hIL-6 stimulation whereas TGF-β did not show enhanced responses
345 (**Fig. 1C, D**). Generally, chronic inflammation leads to a stronger inflammatory response,
346 which is described as immunological training [45]. In immunological training, the primary
347 stimulus will prime specific regulatory elements in enhancer regions. This established
348 chromatin landscape allows faster and increased transcriptional activation of the

349 secondary stimulus, leading to an enhanced inflammatory response. At the chromatin
350 level, immunological training has been shown to induce long-lasting epigenetic
351 remodeling of regulatory elements [46]. This remodeling includes changes in activating
352 histone marks such as H3K27Ac and H3K4me3 [46, 47]. In this study, signal-dependent
353 transcription factors such as STAT1 and STAT3 motifs were enriched at up-regulated
354 gene promoters, and BRD4 and H3K27Ac were increasingly co-occupied at those
355 promoters **(Fig. 2C)**. After removal of the stimulus, STAT3 is likely to be left from the
356 promoters; however, our study suggested that BRD4 and the activated H3K27Ac
357 modification remained and established a "primed" chromatin state for subsequent
358 activation **(Fig. 5)**. As a result, LPS activated selected genes that had been primed by
359 STAT3, more quickly and strongly **(Fig. 4E)**. Indeed, cellular enzymes that are known to
360 be enriched at enhancers such as PU.1, MED1, SWI/SNF complexes are predicted to be
361 co-occupied at newly responding gene promoters **(Fig. 2A, SFig. 2C)**. These
362 observations support that vIL-6 stimulation induced transcription reprogramming, which
363 favors a subsequent inflammation response.

364 What would be the evolutional advantage for maintaining vIL-6 in KSHV genome?
365 Interestingly, vIL-6 is reported to be constitutively expressed in some cell populations
366 even during latent infection [13, 48]. We think that immunological training effects are

367 utilized for the establishment of active latent chromatin for inducible lytic gene expression.
368 Consistent with this hypothesis, BRD4, H3K27Ac, and H3K4me3 are all highly
369 accumulated at the KSHV ori-Lyt region in latent chromatin [49]. We think that KSHV is
370 likely to utilize host defense mechanisms to recruit BRD4 on its genome to establish a
371 "primed" latent chromatin for further reactivation, which is partly seen in increased KSHV
372 transcription in vIL-6/THP-1 cells (**Fig. 1F, G**). Perhaps, related to this, we recently
373 showed that the vIL-6KO virus could not reprogram primary infected monocytes and could
374 not replicate continuously [25]. These cellular and virological vIL-6 functions are likely to
375 contribute to the highly inflammatory phenotypes seen in KSHV-infected patients.
376 In summary, we reported that long-term vIL-6 exposure increased BRD4 and
377 H3K27Ac co-occupancies at inflammatory-related genes, resulting in enhanced
378 inflammatory responses to LPS. BRD4 is clearly the center of the altered cell responses
379 caused by prolonged vIL-6 exposure, in which the pre-located BRD4 on the promoter
380 enabled transcription factors and cofactors that are brought in proximity by p65 to interact
381 more rapidly and steadily upon LPS stimulation. Changes in the enhancer-promoter
382 genomic interactions by long-term exposure to vIL-6 remain a promising avenue for
383 further research. Moreover, animal models with continuous vIL-6 exposure should reveal
384 how vIL-6 trained memory polarizes immune cell communications and react to secondary

385 stimuli, which will provide valuable information for a better understanding the
386 pathogenesis of KICS. Although continued treatment with BET inhibitors is known to
387 cause large genomic structural changes and rapidly induce drug-resistant cells [50, 51],
388 short-term treatment with well-scheduled drug holidays may be beneficial to reverse the
389 immunological training memory established by KSHV vIL-6.

390 **MATERIALS AND METHODS**

391 **Chemicals, reagents and antibodies**

392 Dulbecco's modified minimal essential medium (DMEM), fetal bovine serum (FBS),
393 phosphate-buffered saline (PBS), Trypsin-EDTA solution, 100 X penicillin–streptomycin–
394 L-glutamine solution were purchased from Thermo Fisher (Waltham, MA). Puromycin and
395 G418 solution were obtained from InvivoGen (San Diego, CA). Hygromycin B solution
396 was purchased from Enzo Life Science (Farmingdale, NY).

397 The following antibodies were used for CUT & RUN, immunoblotting and flow cytometry:
398 rabbit anti-BRD4 (Cell Signaling, E2A7X), rabbit anti-RNAPII (Millipore, clone CTD4H8),
399 rabbit anti-H3K27ac (CST, clone D5E4), rabbit anti-H3K4me3 (Cell Signaling, clone
400 C42D8), mouse anti-β-actin (Santa Cruz 47778), rabbit anti-gp130 (CST), rabbit IgG
401 (CST, clone DA1E). Rabbit anti-vIL-6 was a gift from Dr. Robert Yarchoan (NIH/NCI).

402

403 **Cells**

404 THP-1 cell lines was obtained from ATCC. Cells were maintained in an RPMI 1640
405 medium supplemented with 1% fetal bovine serum (FBS; Invitrogen), 2 mM L-glutamine
406 and 100 U/ml penicillin and 100 μg/ml streptomycin at 37°C in a humidified 5% CO_2. THP-
407 1 cells were passaged two to three times per week when reaching 1 x 10^6 cells/ml.

408 **Purification of recombinant protein**

409 *Spodoptera frugiperda* Sf9 cells (Millipore) were maintained in Ex-Cell 420 medium
410 (Sigma), and recombinant baculoviruses were generated with the BAC-to-Bac system as
411 previously described [52] [53].

412

413 **SLAM-seq**

414 SLAM-seq [27] was performed using the SLAMseq Kinetics Kit (Lexogen GmbH, Vienna,
415 Austria) according to the manufacturer's standard protocol.

416 Briefly, biological replicate cultures of THP-1 cells were incubated with vIL-6 (100µg/ml)
417 for 30 min or 2 weeks. Subsequently, 4-Thiouridine (s4U; 300 µM) was added to the
418 culture media and the cells were incubated for 1 h in order to label newly synthesized
419 RNA. As for the LPS (100ng/ml) stimulation, s4U was added to the culture media
420 simultaneously with LPS, and cells were incubated for 6 hours. Total RNA was isolated
421 and then the 4-thiol groups in the s4Uracil-labeled transcripts were alkylated with
422 iodoacetamide (IAA). QuantSeq 3′ mRNA-Seq (FWD) (Lexogen, Inc.) Illumina-compatible,
423 indexed sequencing libraries were prepared from alkylated RNA samples (100 ng)
424 according to the manufacturer's protocol for oligo(dT)-primed first-strand cDNA synthesis,
425 random-primed second-strand synthesis, and library amplification. Libraries were

426 multiplex sequenced (1 × 100 bp, single read) on an Illumina HiSeq 4000 sequencing
427 system. SLAM-Seq datasets were analyzed using the T > C conversion-aware SLAM-
428 DUNK (Digital Unmasking of Nucleotide conversion-containing k-mers) pipeline utilizing
429 the default parameters [27, 54]. Briefly, nucleotide conversion-aware read mapping of
430 adapter- and poly(A)-trimmed sequences to the human GRCh38/hg38 reference genome
431 assembly was performed with NextGenMap [55]. Alignments were filtered for those with
432 a minimum identity of 95% and minimum of 50% of the read bases mapped. For multi-
433 mappers, ambiguous reads and non-3′ UTR alignments were discarded, while one read
434 was randomly selected from multimappers aligned to the same 3′ UTR. SNP calling
435 (coverage cut-off of 10X and variant fraction cut-off of 0.8) with VarScan2 [56] was
436 performed in order to mask actual T > C SNPs. Non-SNP T > C conversion events were
437 then counted and the fraction of labeled transcripts was determined. All results were used
438 for downstream analyses, such as nascent transcript analysis and differential expression
439 analysis (DESeq2) [57].
440

441 **Bioinformatics analysis of SLAM-seq data**

442 The UCSC Genome Browser was used to convert RefSeq IDs to gene symbols (refGene).
443 The resulting data were first filtered by log2 fold change and sorted by adjusted p-value

444 from lowest to highest. The resulting up-regulated genes (log2 fold change >1 and
445 adjusted *p*-value <0.01) were extracted. For functional enrichment analysis (KEGG
446 pathway analysis), the official gene symbols were applied in DAVID web service tools
447 [58]. For transcription factor analysis, gene symbols were submitted to ChIP-Atlas [59] to
448 analyze common regulators and to predict transcription factor binding. The following
449 parameters were used; Organism (annotation): Homo sapiens (hg38), Experiment type;
450 TFs and others, Cell type Class; Blood, Threshold; 100. The output factors were then
451 listed and plotted in a Venn diagram.
452
453 **RNA-sequencing**
454 vIL-6/THP-1 and parental THP-1 cells were infected with or without r219.KSHV for 72h
455 and RNA was purified using the Quick-RNA miniprep kit (Zymo Research, Irvine, CA,
456 USA). Indexed, stranded mRNA-seq libraries were prepared from total RNA (100 ng)
457 using the KAPA Stranded mRNA-Seq kit (Roche) according to the manufacturer's
458 standard protocol. Libraries were pooled and multiplex sequenced on an Illumina
459 NovaSeq 6000 system (150-bp, paired-end, >30 × 106 reads per sample). RNA-Seq data
460 was analyzed using a Salmon-tximport-DESeq2 pipeline. Raw sequence reads (FASTQ
461 format) were mapped to the reference human genome assembly (GRCh38/hg38,

462 GENCODE release 36) and quantified with Salmon [60]. Gene-level counts were
463 imported with tximport [61] and differential expression analysis was performed by
464 DESeq2 [57], which are visualized by Venn diagram.
465

466 **Cleavage under targets and release using nuclease (CUT&RUN)**

467 CUT&RUN [29] was performed essentially by following the online protocol developed by
468 Dr. Henikoff's lab with a few modifications to fit our needs. Cells were washed with PBS
469 and wash buffer [20 mM HEPES-KOH pH 7.5, 150 mM NaCl, 0.5 mM Spermidine (Sigma,
470 S2626), and proteinase inhibitor (Roche)]. After removing the wash buffer, cells were
471 captured on magnetic concanavalin A (ConA) beads (Polysciences, PA, USA) in the
472 presence of CaCl2. Beads/cells complexes were washed three times with digitonin wash
473 buffer (0.02% digitonin, 20 mM HEPES-KOH pH 7.5, 150 mM NaCl, 0.5 mM Spermidine
474 and 1x proteinase inhibitor), aliquoted, and incubated with specific antibodies (1:50) in
475 250 μL volume at 4℃ overnight. After incubation, unbound antibody was removed by
476 washing with digitonin wash buffer three times. Beads were then incubated with
477 recombinant Protein A/G–Micrococcal Nuclease (pAG-MNase), which was purified from
478 E.coli in 250 μl digitonin wash buffer at 1.0 μg/mL final concentration for 1 h at 4 °C with
479 rotation. Unbound pAG-MNase was removed by washing with digitonin wash buffer three

480 times. Pre-chilled digitonin wash buffer containing 2 mM $CaCl_2$ (200 μL) was added to the
481 beads and incubated on ice for 30 min. The pAG-MNase digestion was halted by the
482 addition of 200 μl 2× STOP solution (340 mM NaCl, 20 mM EDTA, 4 mM EGTA, 50 μg/ml
483 RNase A, 50 μg/ml glycogen). The beads were incubated with shaking at 37 °C for 10 min
484 in a tube shaker at 300 rpm to release digested DNA fragments from the insoluble nuclear
485 chromatin. The supernatant was then collected by removing the magnetic beads. DNA in
486 the supernatant was purified using the NucleoSpin Gel & PCR kit (Takara Bio, Kusatsu,
487 Shiga, Japan). Sequencing libraries were then prepared from 3 ng DNA with the Kapa
488 HyperPrep Kit (Roche) according to the manufacturer's standard protocol. Libraries were
489 multiplex sequenced (2 × 150 bp, paired-end) on an Illumina NovaSeq 6000 system to
490 yield ~15 million mapped reads per sample. With separate replicated experiments, qPCR
491 was used to examine enrichment at selected genomic regions. Primer sequences are
492 provided in **Table.S1.**
493 CUT&RUN sequence reads were processed with fastp [62] and aligned to the human
494 GRCh38/hg38 reference genome assembly with Bowtie2 and yielding mapped reads in
495 BAM files [63]. Hypergeometric Optimization of Motif EnRichment (HOMER) v4.11 was
496 used for peak detection and their annotation utilizing the defalt parameters described in
497 the developer's manual [31]. Deeptools was used for making plotprofiles utilizing the

498 defalt parameters [64]. Peaks and read alignments were visualized using the Integrated

499 Genome Browser [65].

500

501 **Olink analysis**

502 1.5 X 10^6 THP-1 cells or vIL-6/THP-1 cells were prepared in triplicate and washed twice

503 by PBS10ml and then suspended with 1ml fresh RPMI medium in 12 well plates.

504 Inflammatory cytokines such as LPS (100ng/ml), IFN α (100ng/ml), vIL-6 (100ng/ml) and

505 hIL-6 (100ng/ml) were then added to each well and cultured at 37℃, 5% CO_2. 6 hours

506 after incubation, supernatants were harvested and centrifuged (3,000 rpm, 3min) to

507 remove the remaining cells. The resulting supernatant samples were stored at -20℃ for

508 approximately two weeks until they were sent for analysis. Samples wrapped in dry ice

509 were then sent to Olink Proteomics (Temple City, CA). Olink's Proximity Extension Assay

510 (PEA) technology uses antibody pairs conjugated to unique oligonucleotides and is

511 quantified via PCR. When both antibodies of a pair bind the target protein simultaneously,

512 their respective conjugated oligonucleotides are brought into proximity, facilitating

513 hybridization. The oligonucleotide sequence is then extended by DNA polymerase,

514 amplified, and measured by qPCR to determine the sample's initial protein abundance.

515 Raw analyte expression values after PCR underwent multiple rounds of transformation

516 by Olink, including a log2 transformation, and were returned as normalized protein
517 expression (NPX) values [66]. For evaluating inflammatory cytokine production in the
518 culture medium, the Olink® Target 48 Cytokine panel was selected by multiple
519 investigators. The data was processed with Olink Insight Stat Analysis software.
520
521 **RT-qPCR**
522 Total RNA was extracted using the Quick-RNA miniprep kit (Zymo Research, Irvine, CA,
523 USA). A total of 1 μg of RNA was incubated with DNase I for 15min and reverse
524 transcribed with the High Capacity cDNA Reverse Transcription Kit (Thermo Fisher,
525 Waltham, MA USA). The resulting cDNA was used for qPCR. 10 μl SYBR Green
526 Universal master mix (Bio-Rad) was used for qPCR according to the manufacturer's
527 instructions. Each sample was normalized to 18S ribosomal RNA, and the ddCt fold
528 change method was used to calculate relative quantification. All reactions were run in
529 triplicate. Primer sequences used for qRT-PCR are provided in the **Table. S1.**
530
531 **Immunoblotting**
532 Cells were washed with PBS, lysed in lysis buffer (50 mM Tris-HCl [pH 6.8], 2% SDS,
533 10% glycerol) and boiled for 3min. The protein concentrations of the lysates were

534 quantified with a BCA Protein Assay Kit (Thermo Fisher). Protein samples were
535 separated by SDS-PAGE using 10% agarose gel and transferred to transfer membranes
536 (Millipore-Sigma, St. Louis, MO, USA), which were incubated in 5% nonfat milk (A600669,
537 Sangon) at room temperature for 2 hours. The membrane was incubated with the primary
538 antibody at 4°C overnight or at room temperature for 2 hours. The membrane was then
539 incubated with horseradish-peroxidase-conjugated secondary antibody or Alexa-647-
540 conjugated secondary antibody at 25°C for 1 hour. For cell fractionation, cells were
541 suspended with hypotonic buffer (20mM Tris-HCl(pH 7.4), 10mM NaCl, 3mM MgCl2,
542 0.5mM DTT and proteinase inhibitor cocktail) for 15min on ice and 0.5% NP-40 was
543 added. Cells were then centrifuged for 10 minutes at 3000rpm to collect the supernatants
544 (cytoplasm fraction). Pellets were washed with PBS 2 times and suspended with protein
545 lysis buffer (nuclear fraction).
546

547 **Flow cytometry**

548 Cells in culture were washed twice with PBS and resuspended in FACS buffer (PBS
549 supplemented with 1% FBS) at $1x10^6$ cells/ml. Cells were then stained for 2 hours at room
550 temperature with the gp130 antibodies (1:1000) followed by Alexa-647-conjugated
551 secondary antibody for 1 hour. For intracellular nuclear staining to measure cell cycle,

552 cells were washed twice with PBS and incubated with propidium iodide (PI) solution
553 (50ng/ml PI, 0.2% NP-40, 0,25mg/ml RNase) for 15 min at 4°C and then for 30 min at
554 37°C in the dark. Flow cytometry was carried out by using a BD Acuri instrument (BD
555 Biosciences) and data analysis was performed using FlowJo v10.8.1 (Tree Star) by gating
556 on live cells based on forward versus side scatter profiles. Cell cycle was calculated by
557 Watson model implemented in FlowJo according to the manufacture's protocol.
558

559 **Capture of nascent RNAs**

560 To capture nascent RNAs, 0.4 mM EdU was added into the culture medium and was
561 incorporated into the cells for 2 hours. Total RNA was prepared with (). The EdU-labeled
562 RNAs were then biotinylated and captured by using the Click-it Nascent RNA Capture Kit
563 (Life Technologies), in accordance with the manufacturer's instructions. Briefly, 1 µg of
564 EU-labeled RNA was biotinylated with 0.5 mM biotin azide in Click-iT reaction buffer. The
565 biotinylated RNAs were precipitated with ethanol at 4°C overnight and resuspended in 50
566 µl distilled water. The biotinylated RNAs were then mixed with 12 µl Dynabeads MyOne
567 Streptavidin T1 magnetic beads in Click-iT RNA binding buffer and heated at 68°C for 5
568 min, followed by incubation at room temperature for 30 min while gently vortexing. The
569 beads were immobilized using the DynaMag-2 magnet and were washed with Click-iT

570 wash buffers 1 and 2. The washed beads were resuspended in Click-iT wash buffer 2
571 and used for cDNA synthesis. cDNA synthesis was performed by the High Capacity cDNA
572 Reverse Transcription Kit as described above.
573

574 **Statistical analysis**

575 Experimental replicates of at least 3 for each sample, including negative controls, were
576 prepared whenever applicable. Results are shown as mean ± SD from at least three
577 independent experiments. Statistical analyses were performed using GraphPad Prism
578 9.4.1 software. Statistical significance was determined by appropriate testing with
579 Student's t-test and one-way ANOVA with Tukey's multiple comparison test. A value of p
580 < 0.05 was considered statistically significant.
581

582 **Data availability**

583 The RNA-seq, SLAMseq, and CUT and RUN data were deposited in NCBI Gene
584 Expression Omnibus (GEO) database under accession numbers; GSE232843,
585 GSE233119, and GSE233323.
586
587

588 **Acknowledgments**

589 We would like to thank Dr. Robert Yarchoan (NIH/NCI) for the generous gift of rabbit
590 monoclonal antibody against vIL-6. We would like to thank the Flow Cytometry and
591 Genomics Shared Resources at the UC Davis Comprehensive Cancer Center for expert
592 support. This research was supported by public health grants from the National Cancer
593 Institute (CA225266, CA232845) and the National Institute of Allergy and Infectious
594 Disease (AI155515 and AI167663) to Y.I. The Genomics and Flow Cytometry Shared
595 Resources are supported by the UC Davis Comprehensive Cancer Center Support Grant
596 (CCSG) awarded by the National Cancer Institute (NCI P30CA093373).

597

598

599 **Figure legends**

600 **Figure 1. Biological effects of prolonged vIL-6 exposure** **(A)** A schematic diagram
601 of the THP-1 cell culture model. THP-1 cells were treated with or without vIL-6 every other
602 day for 2 weeks (THP-1, vIL-6/THP-1). After withdrawal of the cytokine for 24 hours. vIL-
603 6, hIL-6 and TGF-β were added for 30 minutes for secondary stimulation. Subsequently,
604 4-Thiouridine (4sU, 300 μM) was added to the culture media and the cells were incubated
605 for 1 hr to label newly synthesized RNA. Newly synthesized RNA was then alkylated by
606 iodoacetamide (IAA, 100mM). Total RNA was isolated for the following analyses. **(B)**
607 Principal component analysis (PCA). Nascent transcribed gene expression in THP-1 and
608 vIL-6/THP-1 cells was shown. vIL-6, hIL-6 and TGF-β were used as secondary stimulation.
609 Untreated THP-1 cells were used as a control. The samples were represented by three
610 biological replicates. The x and y axes show the percentage of variance explained by PC1
611 (55% variance) and PC2 (22% variance). **(C)** The number of upregulated genes (log2 fold
612 change >1, adj *p*-value < 0.01) after vIL-6 stimulation (left) and TGF-β stimulation (right).
613 Red and green circles represent THP-1 and vIL-6/THP-1 cells, respectively. **(D)**
614 Comparison of up-regulated gene expression between parent THP-1 and vIL-6/THP-1
615 cells after stimulation with vIL-6 (left, N = 344) or TGFβ (right, N = 484). Data were
616 analyzed using Wilcoxon matched-pairs signed ranked test and shown as median. **(E)**

617 KEGG pathway analysis performed on up-regulated genes (log2 fold change >1, adj *p*-
618 value < 0.01) in either THP-1 or vIL-6/THP-1 cells with vIL-6 stimulation. Each bar
619 represents the pathways that were enriched only in parental THP-1 cells (red), only in
620 vIL-6/THP-1 cells (green), or commonly enriched (light green). Results are presented in
621 descending order of the analysis. **(F)** Comparison of all KSHV gene expression between
622 parent THP-1 and vIL-6/THP-1 cells after KSHV infection (N = 88). Data were analyzed
623 using Wilcoxon matched-pairs signed ranked test and shown as median. **(G)** RNA-
624 sequence reads aligned to the KSHV genome (NC 009333.1) in parent THP-1 (red) and
625 vIL-6/THP-1 cells (blue) after KSHV infection.
626
627 **Figure 2. Newly BRD4 recruitment and H3K27Ac translocation in vIl-6/THP-1 cells**
628 **(A)** Enrichment analysis by CHIP-Atlas. Enrichment analysis was performed on the list
629 of genes whose expression were up-regulated by vIL-6 stimulation. The parameters used
630 were as follows; cell type class: blood, threshold for significance: 100, threshold for log10
631 adjusted *p* value < -10. The Venn diagram shows the relatedness and number of genes
632 up-regulated after vIL-6 stimulation in parental THP-1 (red circle) and vIL-6/THP-1 cells
633 (green circle). **(B)** The predicted transcription factors or mediators selectively enriched
634 only in vIL-6/THP-1 cells. The results were limited to THP-1 cells in Chip-Atlas database.

635 **(C)** CUT&RUN signals in ±5-kbp windows around the center of peaks in vIL-6/THP-1 cells.
636 The list of peaks (p-value < 10^{-4}) was extracted using findPeaks (HOMER with default
637 parameters). Enrichment is shown in vIL-6/THP-1 (blue line) and in THP-1 (red line) cells.
638 Images were drawn by plotProfile (HOMER). **(D)** H3K27Ac marks in parental THP-1 and
639 vIL-6/THP-1 cells. The number of H3K27Ac peaks in vIL-6/THP-1 and parental THP-1
640 cells are depicted by a Venn diagram. **(E)** BRD4 CUT&RUN signals in vIL-6/THP-1 cells.
641 The green line indicates BRD4 peaks±5-kbp around the center of H3K27Ac peaks in vIL-
642 6/THP1 cells while the pink line indicates those in parental THP-1 cells. **(F)** Schematic
643 model of H3K27Ac translocation and BRD4 recruitment at newly emerged H3K27Ac
644 regions in vIL-6/THP-1 cells. **(G)** Distances of the nearest TSS to overlapping peaks of
645 BRD4 binding and H3K27Ac enrichment sites. Total peaks counts are shown. *P* values
646 were calculated by the Kolmogorov–Smirnov test. **(H)** Annotation of overlapping peaks
647 between BRD4 and H3K27Ac enrichment sites. Each annotation and its proportion were
648 calculated by annotatePeaks.pl (Homer; parameters; default). Promoter regions are
649 defined as ± 1-kbp from TSS. **(I)** BRD4 CUT&RUN signals in ±5-kbp windows around the
650 center of CTCF peaks in vIL-6/THP-1 cells (blue) and parental THP-1 cells (pink).
651

652 **Figure 3. Prolonged vIL-6 exposure enhances inflammatory response to LPS**
653 **through the novel accumulation of BRD4 and H3K27Ac (A)** Heatmap showing the
654 results of Olink® Target 48 Cytokine panel analysis. LPS (100ng/ml) was added to
655 parental THP-1 or vIL-6/THP-1 cells for 6 hours. Cytokine production in untreated THP-1
656 cells was set as 1 and $\log_2$ fold activation relative to untreated THP-1 cells is shown.
657 Samples were prepared in triplicate and the mean value were shown. **(B)** Individual
658 inflammatory cytokine production determined by Olink proximity extension assay. Data
659 was analyzed using two-sided unpaired Student's *t* test and shown as mean ± SD. **(C)**
660 PCA based on nascent transcribed gene expression in THP-1 cells and vIL-6/THP-1 cells
661 after LPS stimulation. The samples were represented by 3 biological replicates. The x
662 and y axes show the percentage of variance explained by PC1 (98% variance) and PC2
663 (1% variance). **(D)** The number of up-regulated genes (log2 fold change >1, adj *p*-value
664 < 0.01) in THP-1 and vIL-6/THP-1 cells after LPS stimulation (left) and KEGG pathway
665 analysis performed on commonly up-regulated genes (right). **(E)** Schematic diagram for
666 comparing peaks score of up-regulated genes between THP-1 and vIL-6/THP-1 cells.
667 Commonly up-regulated genes by LPS stimulation were obtained from SLAMseq data
668 and BRD4/H3K27Ac merge peaks score were obtained from CUT&RUN data. The peak
669 scores were associated with each up-regulated gene. **(F)** BRD4/H3K27Ac merge peak

670 score for common upregulated genes in THP-1 and vIL-6/THP-1 cells (N = 1626). Data
671 were analyzed using Wilcoxon matched-pairs signed ranked test and shown as median.
672 **(G)** BRD4/H3K27Ac peak score between up-regulated genes (N = 1626) and unchanged
673 genes (log2 fold change >1 and < -1, adj *p*-value > 0.01) (N = 4582) in THP-1 (left) and
674 vIL-6/THP-1 cells (right). Data were analyzed using Mann-Whitney test and shown as
675 median.
676
677 **Figure 4. Association of BRD4 and p65 is responsible for prolonging hIL-6**
678 **transcription burst by LPS** **(A)** Proximity extension assay (PLA) to visualize BRD4 and
679 p65 interaction. THP-1 and vIL-6/THP-1 cells were incubated with LPS (100ng/ml) for 6
680 hours, fixed by 4% PFA/PBS for 15min, permeabilized by 0.15% TritonX/PBS for 10min
681 and PLA was performed. Representative images of PLA (red dots) and quantification of
682 PLA are shown (right). Data were analyzed using a one-way ANOVA test. **(B)**
683 Immunoblotting of p65, H3K27me3 and β-actin in the nuclear and cytoplasmic fractions.
684 THP-1 and vIL-6/THP-1 cells were incubated with LPS (100ng/ml) for 6 hours and cell
685 fractionation was performed. **(C)** The levels of p65 enrichment in the hIL-6, hIL-10 and IL-
686 1β promoter regions were detected using ChIP-qPCR. Normal Rabbit IgG antibody was
687 used as negative control. Data was analyzed using two-sided unpaired Student's *t* test

688 and shown as mean ± SD. **(D)** Nascent RNA expression in THP-1 and vIL-6/THP-1 cells
689 after LPS stimulation. Cells were incubated with LPS and ethynyl uridine (EU) was added
690 0h, 1h 2h, 4h, 8h, 12h after LPS stimulation for 1 hour. Mock samples were prepared
691 without EU for 1 hour incubation with LPS. **(E)** The level of hIL-6, IL-10 and IL-1β gene
692 expression in response to OTX-015 treatment. THP-1 and vIL-6/THP-1 cells were
693 incubated with OTX-015 (10nM) for 4 hours followed by LPS (100ng/ml) for 1 hour. RNA
694 was then collected and transcribed into cDNA for RT-qPCR. 18S rRNA expression was
695 used for internal control. Data were analyzed using a one-way ANOVA test.
696
697 **Figure. 5 Schematic model of transcription reprogramming by prolonged vIL-6**
698 **exposure** Signal-dependent transcription factors such as STAT3 are recruited at up-
699 regulated gene promoters by vIL-6, and BRD4 and H3K27Ac are increasingly co-
700 occupied at those promoters by prolonged vIL-6 exposure. After the removal of the
701 stimulus, STAT3 is removed from the promoters; however, the activated H3K27Ac
702 modification and BRD4 remained and established a "primed" chromatin state for
703 subsequent activation. Subsequent LPS stimulation activated hIL-6 or IL-10 genes that
704 had been primed by vIL-6, more quickly and robustly.
705

706 **References**

707 1. Mizobuchi H, Yamamoto K, Tsutsui S, Yamashita M, Nakata Y, Inagawa H, et al. A unique
708 hybrid characteristic having both pro- and anti-inflammatory phenotype transformed by repetitive
709 low-dose lipopolysaccharide in C8-B4 microglia. Sci Rep. 2020;10(1):8945. Epub 20200602. doi:
710 10.1038/s41598-020-65998-8. PubMed PMID: 32488176; PubMed Central PMCID:
711 PMCPMC7265460.

712 2. Morein D, Rubinstein-Achiasaf L, Brayer H, Dorot O, Pichinuk E, Ben-Yaakov H, et al.
713 Continuous Inflammatory Stimulation Leads via Metabolic Plasticity to a Prometastatic Phenotype
714 in Triple-Negative Breast Cancer Cells. Cells. 2021;10(6). Epub 20210531. doi:
715 10.3390/cells10061356. PubMed PMID: 34072893; PubMed Central PMCID: PMCPMC8229065.

716 3. Ajmone-Cat MA, Nicolini A, Minghetti L. Prolonged exposure of microglia to
717 lipopolysaccharide modifies the intracellular signaling pathways and selectively promotes
718 prostaglandin E2 synthesis. J Neurochem. 2003;87(5):1193-203. doi: 10.1046/j.1471-
719 4159.2003.02087.x. PubMed PMID: 14622099.

720 4. Twayana KS, Chaudhari N, Ravanan P. Prolonged lipopolysaccharide exposure induces
721 transient immunosuppression in BV2 microglia. J Cell Physiol. 2019;234(2):1889-903. Epub
722 20180727. doi: 10.1002/jcp.27064. PubMed PMID: 30054903.

723 5. Chang Y, Cesarman E, Pessin MS, Lee F, Culpepper J, Knowles DM, et al. Identification

724 of herpesvirus-like DNA sequences in AIDS-associated Kaposi's sarcoma. Science.
725 1994;266(5192):1865-9. doi: 10.1126/science.7997879. PubMed PMID: 7997879.
726 6. Antman K, Chang Y. Kaposi's sarcoma. N Engl J Med. 2000;342(14):1027-38. doi:
727 10.1056/NEJM200004063421407. PubMed PMID: 10749966.
728 7. Giffin L, Damania B. KSHV: pathways to tumorigenesis and persistent infection. Adv
729 Virus Res. 2014;88:111-59. doi: 10.1016/B978-0-12-800098-4.00002-7. PubMed PMID:
730 24373311; PubMed Central PMCID: PMCPMC4104069.
731 8. Polizzotto MN, Uldrick TS, Wyvill KM, Aleman K, Marshall V, Wang V, et al. Clinical
732 Features and Outcomes of Patients With Symptomatic Kaposi Sarcoma Herpesvirus (KSHV)-
733 associated Inflammation: Prospective Characterization of KSHV Inflammatory Cytokine
734 Syndrome (KICS). Clin Infect Dis. 2016;62(6):730-8. Epub 2015/12/15. doi: 10.1093/cid/civ996.
735 PubMed PMID: 26658701; PubMed Central PMCID: PMCPMC4772848.
736 9. Chandriani S, Ganem D. Array-based transcript profiling and limiting-dilution reverse
737 transcription-PCR analysis identify additional latent genes in Kaposi's sarcoma-associated
738 herpesvirus. J Virol. 2010;84(11):5565-73. Epub 20100310. doi: 10.1128/JVI.02723-09. PubMed
739 PMID: 20219929; PubMed Central PMCID: PMCPMC2876603.
740 10. Aoki Y, Jaffe ES, Chang Y, Jones K, Teruya-Feldstein J, Moore PS, et al. Angiogenesis
741 and hematopoiesis induced by Kaposi's sarcoma-associated herpesvirus-encoded interleukin-6.

742 Blood. 1999;93(12):4034-43. Epub 1999/06/11. PubMed PMID: 10361100.

743 11. Li W, Wang Q, Qi X, Guo Y, Lu H, Chen Y, et al. Viral interleukin-6 encoded by an
744 oncogenic virus promotes angiogenesis and cellular transformation by enhancing STAT3-
745 mediated epigenetic silencing of caveolin 1. Oncogene. 2020;39(23):4603-18. Epub 20200511.
746 doi: 10.1038/s41388-020-1317-1. PubMed PMID: 32393833; PubMed Central PMCID:
747 PMCPMC7970339.

748 12. Zhu X, Guo Y, Yao S, Yan Q, Xue M, Hao T, et al. Synergy between Kaposi's sarcoma-
749 associated herpesvirus (KSHV) vIL-6 and HIV-1 Nef protein in promotion of angiogenesis and
750 oncogenesis: role of the AKT signaling pathway. Oncogene. 2014;33(15):1986-96. Epub
751 20130422. doi: 10.1038/onc.2013.136. PubMed PMID: 23604117.

752 13. Giffin L, West JA, Damania B. Kaposi's Sarcoma-Associated Herpesvirus Interleukin-6
753 Modulates Endothelial Cell Movement by Upregulating Cellular Genes Involved in Migration. mBio.
754 2015;6(6):e01499-15. Epub 20151208. doi: 10.1128/mBio.01499-15. PubMed PMID: 26646010;
755 PubMed Central PMCID: PMCPMC4676281.

756 14. Fullwood RA, Low GM, Chase EP, Grasley M, Beal SS, McCrary IM, et al. The Kaposi's
757 sarcoma-associated herpesvirus viral interleukin 6 gene affects metastasis and expression of B
758 cell markers in a murine xenograft model. PLoS One. 2018;13(9):e0204947. Epub 20180928. doi:
759 10.1371/journal.pone.0204947. PubMed PMID: 30265712; PubMed Central PMCID:

760 PMCPMC6161906.

761 15. Yadav A, Kalita A, Dhillon S, Banerjee K. JAK/STAT3 pathway is involved in survival of
762 neurons in response to insulin-like growth factor and negatively regulated by suppressor of
763 cytokine signaling-3. J Biol Chem. 2005;280(36):31830-40. Epub 20050705. doi:
764 10.1074/jbc.M501316200. PubMed PMID: 15998644.

765 16. Haura EB, Turkson J, Jove R. Mechanisms of disease: Insights into the emerging role of
766 signal transducers and activators of transcription in cancer. Nat Clin Pract Oncol. 2005;2(6):315-
767 24. doi: 10.1038/ncponc0195. PubMed PMID: 16264989.

768 17. Yu H, Jove R. The STATs of cancer--new molecular targets come of age. Nat Rev Cancer.
769 2004;4(2):97-105. doi: 10.1038/nrc1275. PubMed PMID: 14964307.

770 18. Hirano T. IL-6 in inflammation, autoimmunity and cancer. Int Immunol. 2021;33(3):127-
771 48. doi: 10.1093/intimm/dxaa078. PubMed PMID: 33337480; PubMed Central PMCID:
772 PMCPMC7799025.

773 19. Fu B, Xu X, Wei H. Why tocilizumab could be an effective treatment for severe COVID-
774 19? J Transl Med. 2020;18(1):164. doi: 10.1186/s12967-020-02339-3. PubMed PMID: 32290839;
775 PubMed Central PMCID: PMCPMC7154566.

776 20. Ramaswami R, Lurain K, Peer CJ, Serquina A, Wang V, Widell A, et al. Tocilizumab in
777 patients with symptomatic Kaposi sarcoma herpesvirus-associated multicentric Castleman

778 disease. Blood. 2020;135(25):2316-9. doi: 10.1182/blood.2019004602. PubMed PMID:
779 32276276; PubMed Central PMCID: PMCPMC7316216.
780 21. Nord JA, Wynia-Smith SL, Gehant AL, Jones Lipinski RA, Naatz A, Rioja I, et al. N-
781 terminal BET bromodomain inhibitors disrupt a BRD4-p65 interaction and reduce inducible nitric
782 oxide synthase transcription in pancreatic beta-cells. Front Endocrinol (Lausanne).
783 2022;13:923925. Epub 20220913. doi: 10.3389/fendo.2022.923925. PubMed PMID: 36176467;
784 PubMed Central PMCID: PMCPMC9513428.
785 22. Huang B, Yang XD, Zhou MM, Ozato K, Chen LF. Brd4 coactivates transcriptional
786 activation of NF-kappaB via specific binding to acetylated RelA. Mol Cell Biol. 2009;29(5):1375-
787 87. Epub 2008/12/24. doi: 10.1128/MCB.01365-08. PubMed PMID: 19103749; PubMed Central
788 PMCID: PMCPMC2643823.
789 23. Sabari BR, Dall'Agnese A, Boija A, Klein IA, Coffey EL, Shrinivas K, et al. Coactivator
790 condensation at super-enhancers links phase separation and gene control. Science.
791 2018;361(6400). Epub 2018/06/23. doi: 10.1126/science.aar3958. PubMed PMID: 29930091;
792 PubMed Central PMCID: PMCPMC6092193.
793 24. Parravicini C, Corbellino M, Paulli M, Magrini U, Lazzarino M, Moore PS, et al.
794 Expression of a virus-derived cytokine, KSHV vIL-6, in HIV-seronegative Castleman's disease.
795 Am J Pathol. 1997;151(6):1517-22. PubMed PMID: 9403701; PubMed Central PMCID:

796 PMCPMC1858372.

797 25. Shimoda M, Inagaki T, Davis R, Merleev A, Tepper CG, Maverakis E, et al. KSHV uses
798 viral IL6 to expand infected immunosuppressive macrophages. bioRxiv. 2023. Epub 2023/03/23.
799 doi: 10.1101/2023.03.05.531224. PubMed PMID: 36945595; PubMed Central PMCID:
800 PMCPMC10028810.

801 26. Shi C, Pamer EG. Monocyte recruitment during infection and inflammation. Nat Rev
802 Immunol. 2011;11(11):762-74. Epub 2011/10/11. doi: 10.1038/nri3070. PubMed PMID: 21984070;
803 PubMed Central PMCID: PMCPMC3947780.

804 27. Herzog VA, Reichholf B, Neumann T, Rescheneder P, Bhat P, Burkard TR, et al. Thiol-
805 linked alkylation of RNA to assess expression dynamics. Nat Methods. 2017;14(12):1198-204.
806 Epub 2017/09/26. doi: 10.1038/nmeth.4435. PubMed PMID: 28945705; PubMed Central PMCID:
807 PMCPMC5712218.

808 28. Kanno T, Kanno Y, LeRoy G, Campos E, Sun HW, Brooks SR, et al. BRD4 assists
809 elongation of both coding and enhancer RNAs by interacting with acetylated histones. Nat Struct
810 Mol Biol. 2014;21(12):1047-57. Epub 20141110. doi: 10.1038/nsmb.2912. PubMed PMID:
811 25383670; PubMed Central PMCID: PMCPMC4720983.

812 29. Skene PJ, Henikoff S. An efficient targeted nuclease strategy for high-resolution mapping
813 of DNA binding sites. Elife. 2017;6. Epub 2017/01/13. doi: 10.7554/eLife.21856. PubMed PMID:

814 28079019; PubMed Central PMCID: PMCPMC5310842.

815 30. Aoki Y, Feldman GM, Tosato G. Inhibition of STAT3 signaling induces apoptosis and
816 decreases survivin expression in primary effusion lymphoma. Blood. 2003;101(4):1535-42. Epub
817 2002/10/24. doi: 10.1182/blood-2002-07-2130. PubMed PMID: 12393476.

818 31. Grossmann C, Ganem D. Effects of NFkappaB activation on KSHV latency and lytic
819 reactivation are complex and context-dependent. Virology. 2008;375(1):94-102. Epub 20080305.
820 doi: 10.1016/j.virol.2007.12.044. PubMed PMID: 18321555; PubMed Central PMCID:
821 PMCPMC2822626.

822 32. Lundberg M, Eriksson A, Tran B, Assarsson E, Fredriksson S. Homogeneous antibody-
823 based proximity extension assays provide sensitive and specific detection of low-abundant
824 proteins in human blood. Nucleic Acids Res. 2011;39(15):e102. Epub 20110606. doi:
825 10.1093/nar/gkr424. PubMed PMID: 21646338; PubMed Central PMCID: PMCPMC3159481.

826 33. Han X, Yu D, Gu R, Jia Y, Wang Q, Jaganathan A, et al. Roles of the BRD4 short isoform
827 in phase separation and active gene transcription. Nat Struct Mol Biol. 2020;27(4):333-41. Epub
828 20200316. doi: 10.1038/s41594-020-0394-8. PubMed PMID: 32203489.

829 34. Mullberg J, Geib T, Jostock T, Hoischen SH, Vollmer P, Voltz N, et al. IL-6 receptor
830 independent stimulation of human gp130 by viral IL-6. J Immunol. 2000;164(9):4672-7. doi:
831 10.4049/jimmunol.164.9.4672. PubMed PMID: 10779772.

832 35. Chow D, He X, Snow AL, Rose-John S, Garcia KC. Structure of an extracellular gp130
833 cytokine receptor signaling complex. Science. 2001;291(5511):2150-5. doi:
834 10.1126/science.1058308. PubMed PMID: 11251120.
835 36. Mizobuchi H, Yamamoto K, Tsutsui S, Yamashita M, Nakata Y, Inagawa H, et al. A unique
836 hybrid characteristic having both pro- and anti-inflammatory phenotype transformed by repetitive
837 low-dose lipopolysaccharide in C8-B4 microglia. Scientific Reports. 2020;10(1). doi:
838 10.1038/s41598-020-65998-8.
839 37. Boulanger MJ, Chow DC, Brevnova EE, Garcia KC. Hexameric structure and assembly
840 of the interleukin-6/IL-6 alpha-receptor/gp130 complex. Science. 2003;300(5628):2101-4. doi:
841 10.1126/science.1083901. PubMed PMID: 12829785.
842 38. Heinrich PC, Behrmann I, Muller-Newen G, Schaper F, Graeve L. Interleukin-6-type
843 cytokine signalling through the gp130/Jak/STAT pathway. Biochem J. 1998;334 (Pt 2)(Pt 2):297-
844 314. Epub 1998/08/26. doi: 10.1042/bj3340297. PubMed PMID: 9716487; PubMed Central
845 PMCID: PMCPMC1219691.
846 39. Boulanger MJ, Chow DC, Brevnova E, Martick M, Sandford G, Nicholas J, et al.
847 Molecular mechanisms for viral mimicry of a human cytokine: activation of gp130 by HHV-8
848 interleukin-6. J Mol Biol. 2004;335(2):641-54. Epub 2003/12/16. doi: 10.1016/j.jmb.2003.10.070.
849 PubMed PMID: 14672670.

850 40. Meads MB, Medveczky PG. Kaposi's sarcoma-associated herpesvirus-encoded viral
851 interleukin-6 is secreted and modified differently than human interleukin-6: evidence for a unique
852 autocrine signaling mechanism. J Biol Chem. 2004;279(50):51793-803. Epub 2004/07/20. doi:
853 10.1074/jbc.M407382200. PubMed PMID: 15258150.
854 41. Hu F, Nicholas J. Signal transduction by human herpesvirus 8 viral interleukin-6 (vIL-6)
855 is modulated by the nonsignaling gp80 subunit of the IL-6 receptor complex and is distinct from
856 signaling induced by human IL-6. J Virol. 2006;80(21):10874-8. Epub 2006/09/08. doi:
857 10.1128/JVI.00767-06. PubMed PMID: 16956953; PubMed Central PMCID: PMCPMC1641745.
858 42. Osborne J, Moore PS, Chang Y. KSHV-encoded viral IL-6 activates multiple human IL-6
859 signaling pathways. Hum Immunol. 1999;60(10):921-7. Epub 1999/11/24. doi: 10.1016/s0198-
860 8859(99)00083-x. PubMed PMID: 10566591.
861 43. Chen D, Choi YB, Sandford G, Nicholas J. Determinants of secretion and intracellular
862 localization of human herpesvirus 8 interleukin-6. J Virol. 2009;83(13):6874-82. Epub 2009/04/24.
863 doi: 10.1128/JVI.02625-08. PubMed PMID: 19386721; PubMed Central PMCID:
864 PMCPMC2698573.
865 44. Chen D, Sandford G, Nicholas J. Intracellular signaling mechanisms and activities of
866 human herpesvirus 8 interleukin-6. J Virol. 2009;83(2):722-33. Epub 2008/11/07. doi:
867 10.1128/JVI.01517-08. PubMed PMID: 18987143; PubMed Central PMCID: PMCPMC2612405.

868 45. Schultze JL, Schmieder A, Goerdt S. Macrophage activation in human diseases. Semin
869 Immunol. 2015;27(4):249-56. Epub 20150822. doi: 10.1016/j.smim.2015.07.003. PubMed PMID:
870 26303100.
871 46. Novakovic B, Habibi E, Wang SY, Arts RJW, Davar R, Megchelenbrink W, et al. beta-
872 Glucan Reverses the Epigenetic State of LPS-Induced Immunological Tolerance. Cell.
873 2016;167(5):1354-68 e14. doi: 10.1016/j.cell.2016.09.034. PubMed PMID: 27863248; PubMed
874 Central PMCID: PMCPMC5927328.
875 47. Saeed S, Quintin J, Kerstens HH, Rao NA, Aghajanirefah A, Matarese F, et al. Epigenetic
876 programming of monocyte-to-macrophage differentiation and trained innate immunity. Science.
877 2014;345(6204):1251086. doi: 10.1126/science.1251086. PubMed PMID: 25258085; PubMed
878 Central PMCID: PMCPMC4242194.
879 48. Moore PS, Boshoff C, Weiss RA, Chang Y. Molecular mimicry of human cytokine and
880 cytokine response pathway genes by KSHV. Science. 1996;274(5293):1739-44. doi:
881 10.1126/science.274.5293.1739. PubMed PMID: 8939871.
882 49. Kumar A, Lyu Y, Yanagihashi Y, Chantarasrivong C, Majerciak V, Salemi M, et al. KSHV
883 episome tethering sites on host chromosomes and regulation of latency-lytic switch by CHD4.
884 Cell Rep. 2022;39(6):110788. doi: 10.1016/j.celrep.2022.110788. PubMed PMID: 35545047;
885 PubMed Central PMCID: PMCPMC9153692.

886 50. Fong CY, Gilan O, Lam EY, Rubin AF, Ftouni S, Tyler D, et al. BET inhibitor resistance
887 emerges from leukaemia stem cells. Nature. 2015;525(7570):538-42. Epub 20150914. doi:
888 10.1038/nature14888. PubMed PMID: 26367796; PubMed Central PMCID: PMCPMC6069604.
889 51. Zhou S, Zhang S, Wang L, Huang S, Yuan Y, Yang J, et al. BET protein inhibitor JQ1
890 downregulates chromatin accessibility and suppresses metastasis of gastric cancer via
891 inactivating RUNX2/NID1 signaling. Oncogenesis. 2020;9(3):33. Epub 20200310. doi:
892 10.1038/s41389-020-0218-z. PubMed PMID: 32157097; PubMed Central PMCID:
893 PMCPMC7064486.
894 52. Izumiya Y, Izumiya C, Hsia D, Ellison TJ, Luciw PA, Kung HJ. NF-kappaB serves as a
895 cellular sensor of Kaposi's sarcoma-associated herpesvirus latency and negatively regulates K-
896 Rta by antagonizing the RBP-Jkappa coactivator. J Virol. 2009;83(9):4435-46. Epub 2009/02/27.
897 doi: 10.1128/JVI.01999-08. PubMed PMID: 19244329; PubMed Central PMCID:
898 PMCPMC2668470.
899 53. Kim KY, Huerta SB, Izumiya C, Wang DH, Martinez A, Shevchenko B, et al. Kaposi's
900 sarcoma-associated herpesvirus (KSHV) latency-associated nuclear antigen regulates the KSHV
901 epigenome by association with the histone demethylase KDM3A. J Virol. 2013;87(12):6782-93.
902 Epub 2013/04/12. doi: 10.1128/JVI.00011-13. PubMed PMID: 23576503; PubMed Central
903 PMCID: PMCPMC3676133.

904 54. Neumann T, Herzog VA, Muhar M, von Haeseler A, Zuber J, Ameres SL, et al.
905 Quantification of experimentally induced nucleotide conversions in high-throughput sequencing
906 datasets. BMC Bioinformatics. 2019;20(1):258. Epub 20190520. doi: 10.1186/s12859-019-2849-
907 7. PubMed PMID: 31109287; PubMed Central PMCID: PMCPMC6528199.
908 55. Sedlazeck FJ, Rescheneder P, von Haeseler A. NextGenMap: fast and accurate read
909 mapping in highly polymorphic genomes. Bioinformatics. 2013;29(21):2790-1. Epub 20130823.
910 doi: 10.1093/bioinformatics/btt468. PubMed PMID: 23975764.
911 56. Koboldt DC, Zhang Q, Larson DE, Shen D, McLellan MD, Lin L, et al. VarScan 2: somatic
912 mutation and copy number alteration discovery in cancer by exome sequencing. Genome Res.
913 2012;22(3):568-76. Epub 20120202. doi: 10.1101/gr.129684.111. PubMed PMID: 22300766;
914 PubMed Central PMCID: PMCPMC3290792.
915 57. Love MI, Huber W, Anders S. Moderated estimation of fold change and dispersion for
916 RNA-seq data with DESeq2. Genome Biol. 2014;15(12):550. doi: 10.1186/s13059-014-0550-8.
917 PubMed PMID: 25516281; PubMed Central PMCID: PMCPMC4302049.
918 58. Sherman BT, Hao M, Qiu J, Jiao X, Baseler MW, Lane HC, et al. DAVID: a web server
919 for functional enrichment analysis and functional annotation of gene lists (2021 update). Nucleic
920 Acids Res. 2022;50(W1):W216-21. Epub 20220323. doi: 10.1093/nar/gkac194. PubMed PMID:
921 35325185; PubMed Central PMCID: PMCPMC9252805.

922 59. Zou Z, Ohta T, Miura F, Oki S. ChIP-Atlas 2021 update: a data-mining suite for exploring
923 epigenomic landscapes by fully integrating ChIP-seq, ATAC-seq and Bisulfite-seq data. Nucleic
924 Acids Res. 2022;50(W1):W175-82. Epub 20220324. doi: 10.1093/nar/gkac199. PubMed PMID:
925 35325188; PubMed Central PMCID: PMCPMC9252733.
926 60. Patro R, Duggal G, Love MI, Irizarry RA, Kingsford C. Salmon provides fast and bias-
927 aware quantification of transcript expression. Nat Methods. 2017;14(4):417-9. Epub 20170306.
928 doi: 10.1038/nmeth.4197. PubMed PMID: 28263959; PubMed Central PMCID:
929 PMCPMC5600148.
930 61. Soneson C, Love MI, Robinson MD. Differential analyses for RNA-seq: transcript-level
931 estimates improve gene-level inferences. F1000Res. 2015;4:1521. Epub 20151230. doi:
932 10.12688/f1000research.7563.2. PubMed PMID: 26925227; PubMed Central PMCID:
933 PMCPMC4712774.
934 62. Chen S, Zhou Y, Chen Y, Gu J. fastp: an ultra-fast all-in-one FASTQ preprocessor.
935 Bioinformatics. 2018;34(17):i884-i90. doi: 10.1093/bioinformatics/bty560. PubMed PMID:
936 30423086; PubMed Central PMCID: PMCPMC6129281.
937 63. Langmead B, Salzberg SL. Fast gapped-read alignment with Bowtie 2. Nat Methods.
938 2012;9(4):357-9. Epub 20120304. doi: 10.1038/nmeth.1923. PubMed PMID: 22388286; PubMed
939 Central PMCID: PMCPMC3322381.

940 64. Ramirez F, Ryan DP, Gruning B, Bhardwaj V, Kilpert F, Richter AS, et al. deepTools2: a
941 next generation web server for deep-sequencing data analysis. Nucleic Acids Res.
942 2016;44(W1):W160-5. Epub 20160413. doi: 10.1093/nar/gkw257. PubMed PMID: 27079975;
943 PubMed Central PMCID: PMCPMC4987876.
944 65. Freese NH, Norris DC, Loraine AE. Integrated genome browser: visual analytics platform
945 for genomics. Bioinformatics. 2016;32(14):2089-95. Epub 20160316. doi:
946 10.1093/bioinformatics/btw069. PubMed PMID: 27153568; PubMed Central PMCID:
947 PMCPMC4937187.
948 66. Assarsson E, Lundberg M, Holmquist G, Bjorkesten J, Thorsen SB, Ekman D, et al.
949 Homogenous 96-plex PEA immunoassay exhibiting high sensitivity, specificity, and excellent
950 scalability. PLoS One. 2014;9(4):e95192. Epub 20140422. doi: 10.1371/journal.pone.0095192.
951 PubMed PMID: 24755770; PubMed Central PMCID: PMCPMC3995906.
952
953

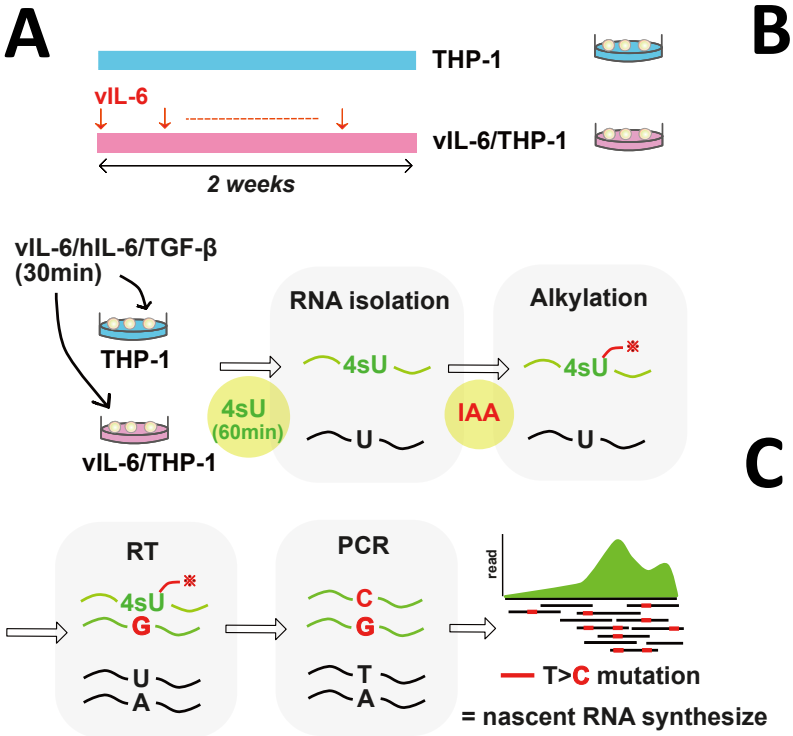
A
THP-1
vIL-6
vIL-6/THP-1
2 weeks
vIL-6/hIL-6/TGF-β
(30min)
THP-1
vIL-6/THP-1
4sU
(60min)
RNA isolation
4sU
U
IAA
Alkylation
4sU
U
RT
4sU
G
U
A
PCR
C
G
T
A
read
T>C mutation
= nascent RNA synthesize

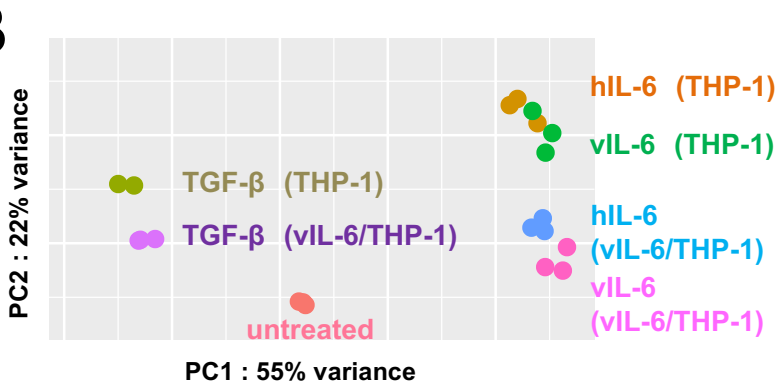
B
hIL-6 (THP-1)
vIL-6 (THP-1)
TGF-β (THP-1)
TGF-β (vIL-6/THP-1)
hIL-6
(vIL-6/THP-1)
vIL-6
(vIL-6/THP-1)
untreated
PC2 : 22% variance
PC1 : 55% variance

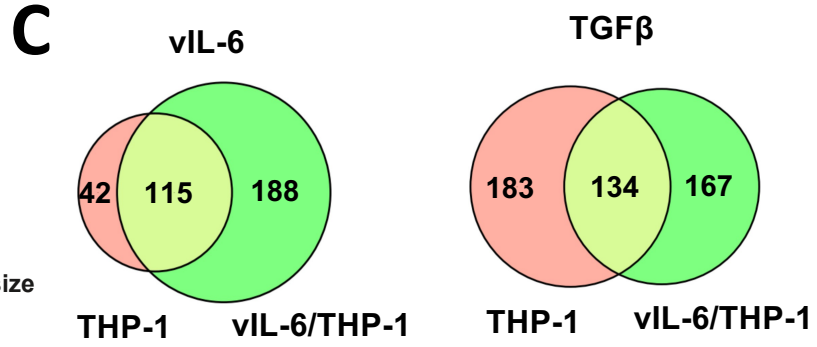
C
vIL-6
42
115
188
THP-1
vIL-6/THP-1
TGFβ
183
134
167
THP-1
vIL-6/THP-1

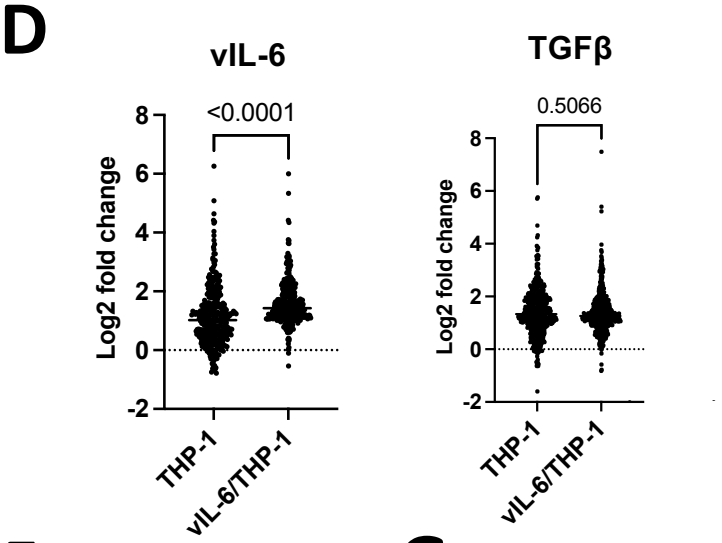
D
vIL-6
<0.0001
Log2 fold change
THP-1
vIL-6/THP-1
TGFβ
0.5066
Log2 fold change
THP-1
vIL-6/THP-1

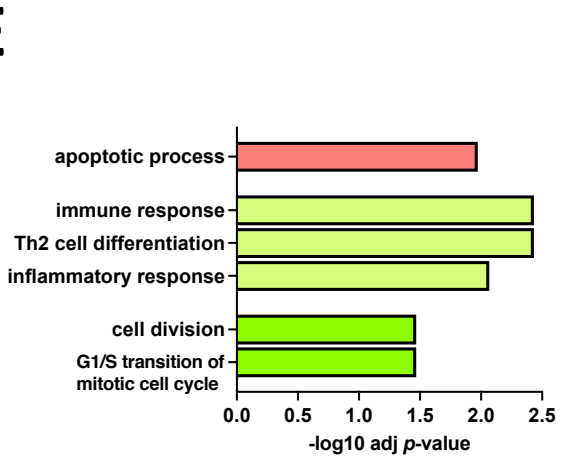
E
apoptotic process
immune response
Th2 cell differentiation
inflammatory response
cell division
G1/S transition of
mitotic cell cycle
-log10 adj p-value

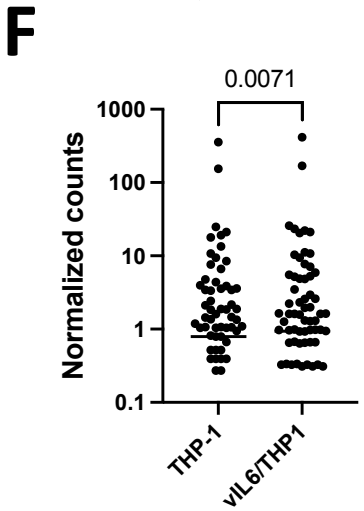
F
0.0071
Normalized counts
THP-1
vIL6/THP1

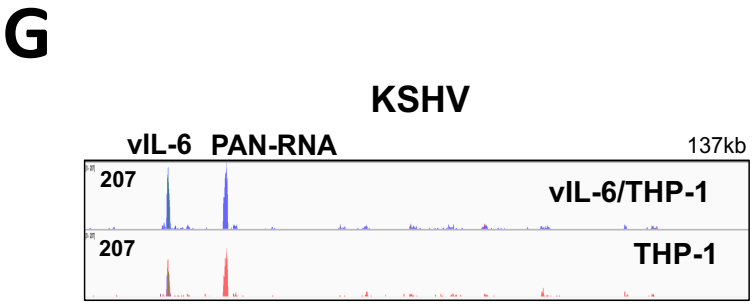
G
KSHV
vIL-6 PAN-RNA
137kb
207
vIL-6/THP-1
207
THP-1

Figure 1

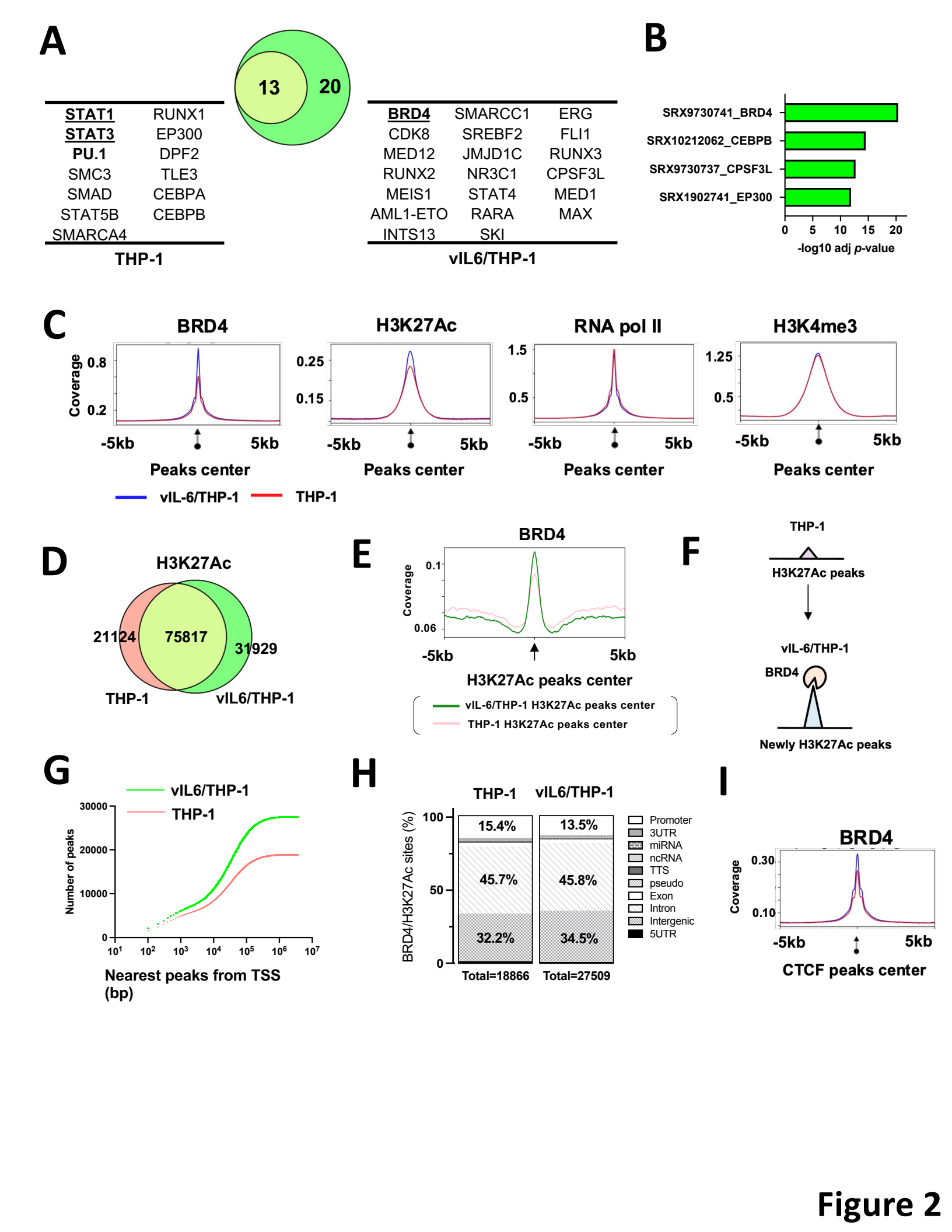
A
13
20
STAT1
STAT3
PU.1
SMC3
SMAD
STAT5B
SMARCA4
RUNX1
EP300
DPF2
TLE3
CEBPA
CEBPB
THP-1
BRD4
CDK8
MED12
RUNX2
MEIS1
AML1-ETO
INTS13
SMARCC1
SREBF2
JMJD1C
NR3C1
STAT4
RARA
SKI
ERG
FLI1
RUNX3
CPSF3L
MED1
MAX
vIL6/THP-1
B
SRX9730741_BRD4
SRX10212062_CEBPB
SRX9730737_CPSF3L
SRX1902741_EP300
0
5
10
15
20
-log10 adj p-value
C
BRD4
H3K27Ac
RNA pol II
H3K4me3
Coverage
0.8
0.2
0.25
0.15
1.5
0.5
1.25
0.5
-5kb
5kb
Peaks center
vIL-6/THP-1
THP-1
D
H3K27Ac
21124
75817
31929
THP-1
vIL6/THP-1
E
BRD4
Coverage
0.1
0.06
-5kb
5kb
H3K27Ac peaks center
vIL-6/THP-1 H3K27Ac peaks center
THP-1 H3K27Ac peaks center
F
THP-1
H3K27Ac peaks
vIL-6/THP-1
BRD4
Newly H3K27Ac peaks
G
vIL6/THP-1
THP-1
Number of peaks
30000
20000
10000
0
10^1
10^2
10^3
10^4
10^5
10^6
10^7
Nearest peaks from TSS (bp)
H
THP-1
vIL6/THP-1
BRD4/H3K27Ac sites (%)
100
50
0
15.4%
45.7%
32.2%
13.5%
45.8%
34.5%
Total=18866
Total=27509
Promoter
3UTR
miRNA
ncRNA
TTS
pseudo
Exon
Intron
Intergenic
5UTR
I
BRD4
Coverage
0.30
0.10
-5kb
5kb
CTCF peaks center

Figure 2

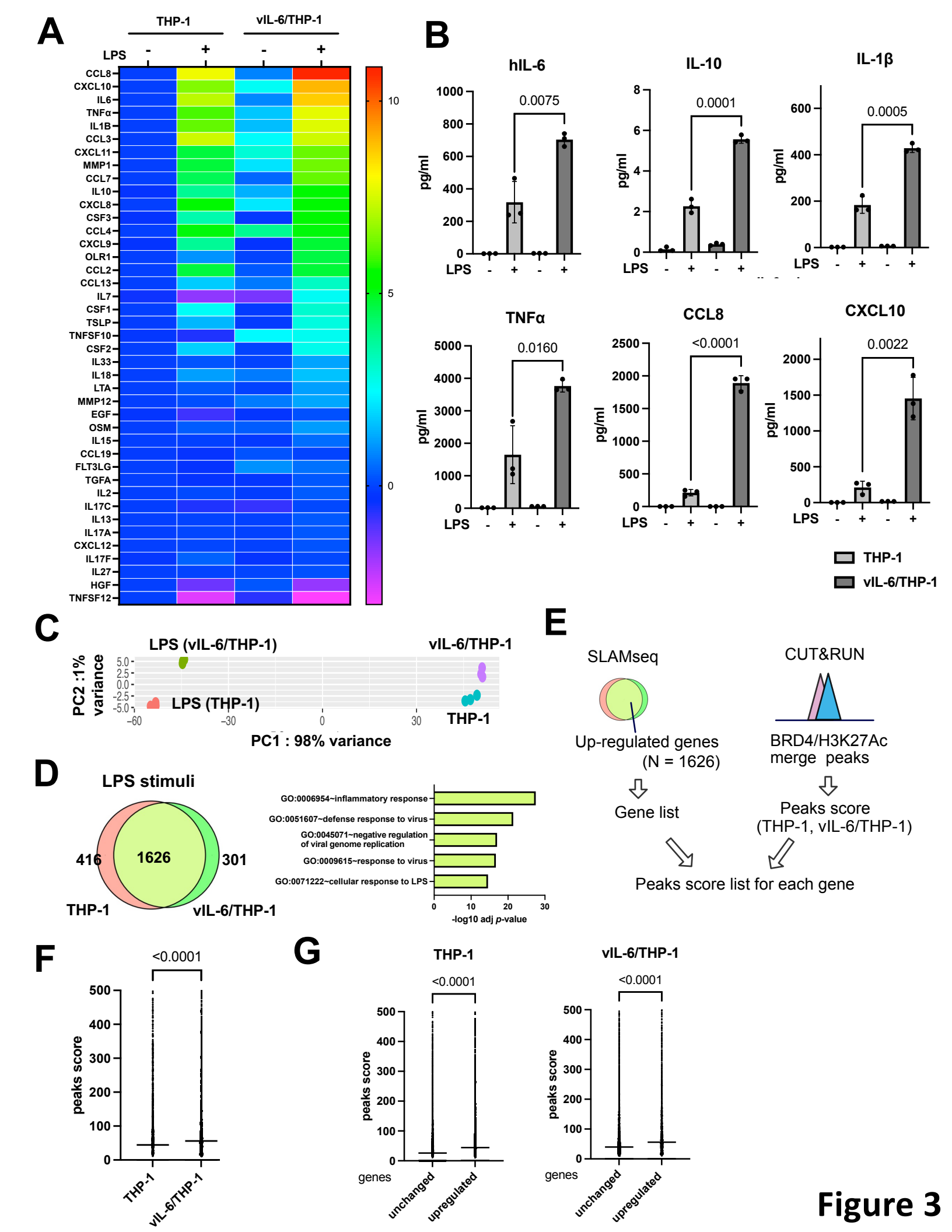
A
THP-1
vIL-6/THP-1
LPS
CCL8
CXCL10
IL6
TNFα
IL1B
CCL3
CXCL11
MMP1
CCL7
IL10
CXCL8
CSF3
CCL4
CXCL9
OLR1
CCL2
CCL13
IL7
CSF1
TSLP
TNFSF10
CSF2
IL33
IL18
LTA
MMP12
EGF
OSM
IL15
CCL19
FLT3LG
TGFA
IL2
IL17C
IL13
IL17A
CXCL12
IL17F
IL27
HGF
TNFSF12
B
hIL-6
0.0075
IL-10
0.0001
IL-1β
0.0005
TNFα
0.0160
CCL8
<0.0001
CXCL10
0.0022
pg/ml
LPS
THP-1
vIL-6/THP-1
C
LPS (vIL-6/THP-1)
vIL-6/THP-1
LPS (THP-1)
THP-1
PC2 :1% variance
PC1 : 98% variance
D
LPS stimuli
416
1626
301
THP-1
vIL-6/THP-1
GO:0006954~inflammatory response
GO:0051607~defense response to virus
GO:0045071~negative regulation of viral genome replication
GO:0009615~response to virus
GO:0071222~cellular response to LPS
-log10 adj p-value
E
SLAMseq
Up-regulated genes
(N = 1626)
Gene list
CUT&RUN
BRD4/H3K27Ac
merge peaks
Peaks score
(THP-1, vIL-6/THP-1)
Peaks score list for each gene
F
<0.0001
peaks score
THP-1
vIL-6/THP-1
G
THP-1
vIL-6/THP-1
<0.0001
genes
unchanged
upregulated

Figure 3

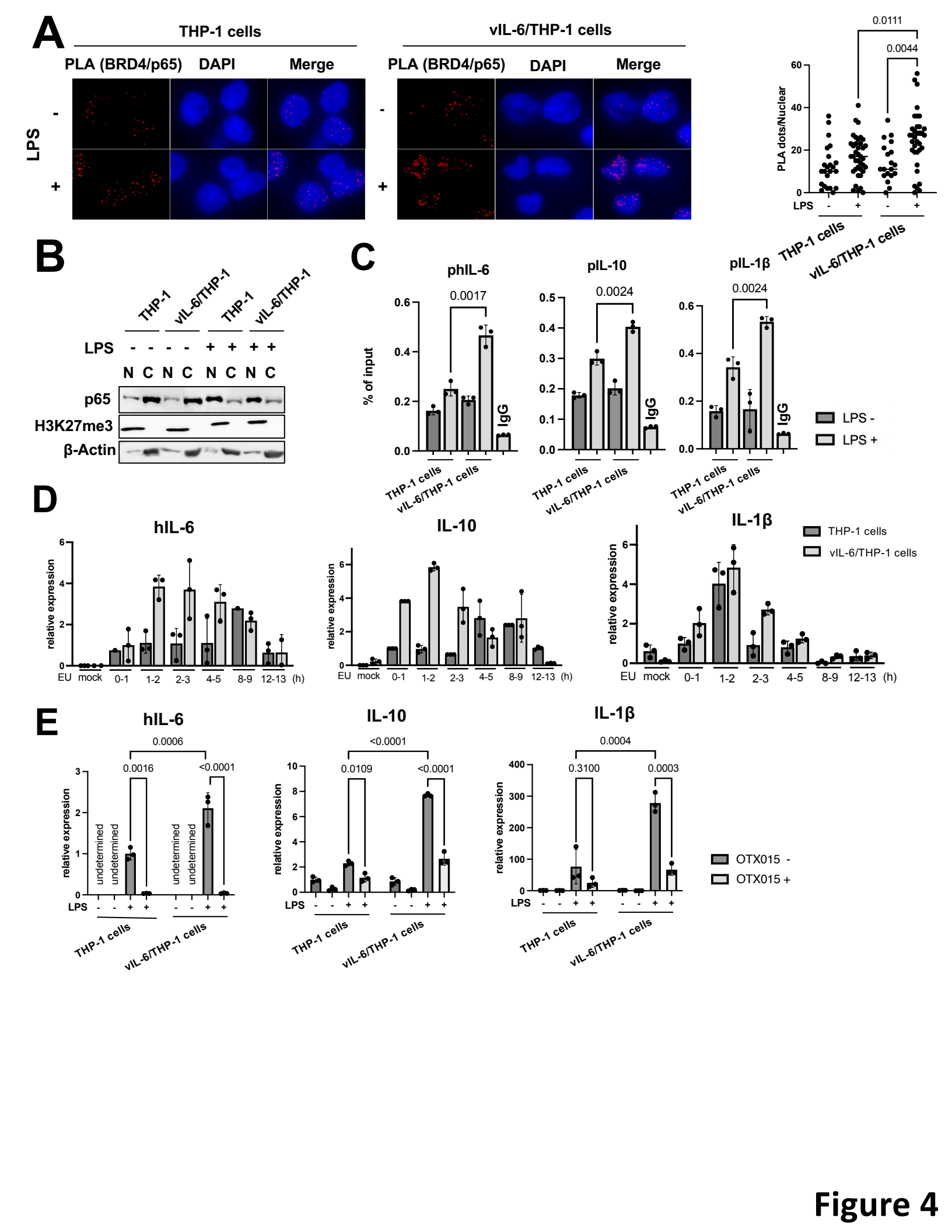
A
THP-1 cells
vIL-6/THP-1 cells
PLA (BRD4/p65)
DAPI
Merge
LPS
-
+
PLA dots/Nuclear
0.0111
0.0044
B
THP-1
vIL-6/THP-1
LPS
N C N C N C N C
p65
H3K27me3
β-Actin
C
phIL-6
pIL-10
pIL-1β
% of input
0.0017
0.0024
0.0024
IgG
LPS -
LPS +
D
hIL-6
IL-10
IL-1β
relative expression
THP-1 cells
vIL-6/THP-1 cells
EU mock 0-1 1-2 2-3 4-5 8-9 12-13 (h)
E
hIL-6
IL-10
IL-1β
0.0006
0.0016
<0.0001
0.0109
<0.0001
0.0004
0.3100
0.0003
undetermined
OTX015 -
OTX015 +

Figure 4

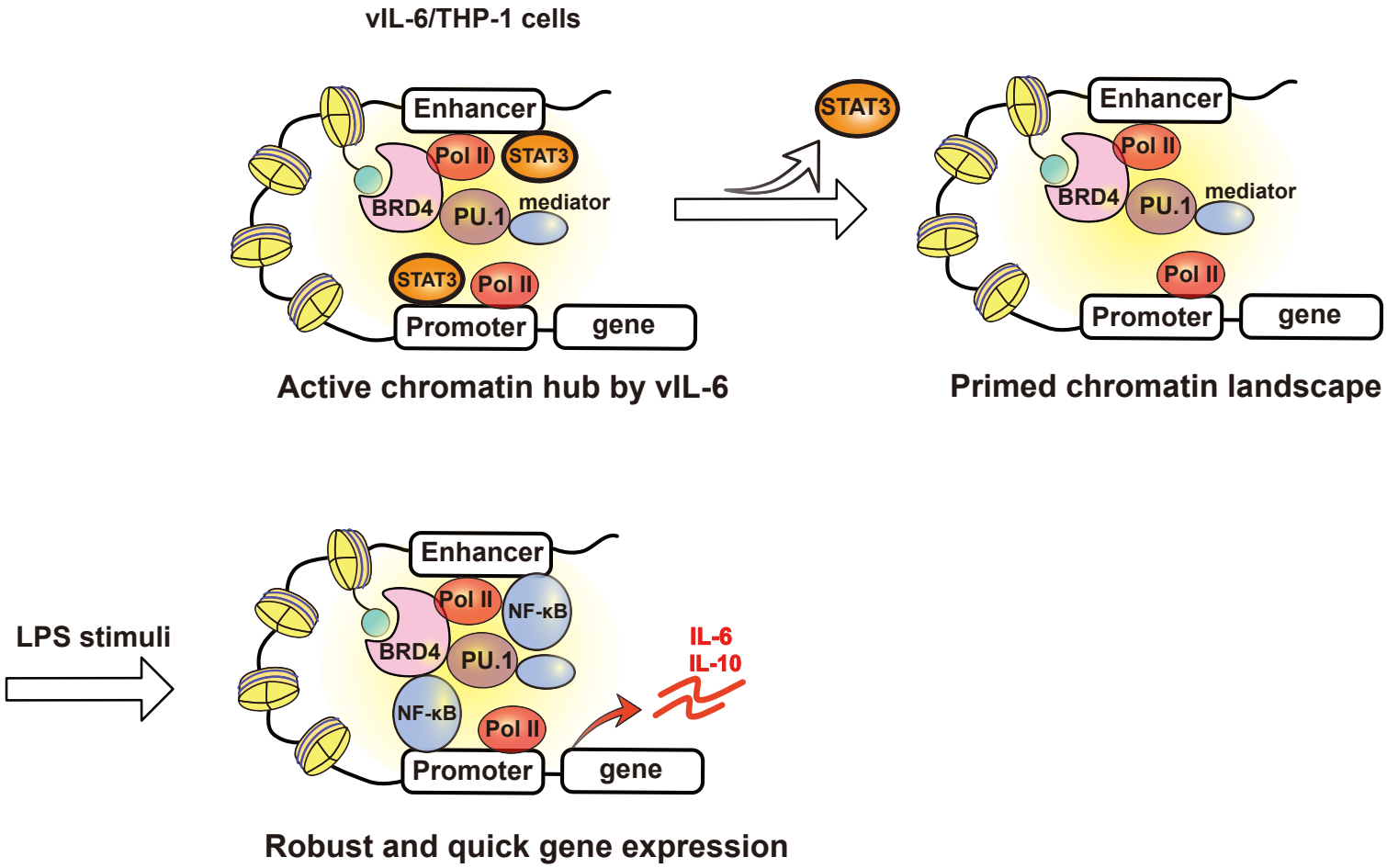
vIL-6/THP-1 cells
Enhancer
Pol II
STAT3
BRD4
PU.1
mediator
STAT3
Pol II
Promoter
gene
Active chromatin hub by vIL-6
STAT3
Enhancer
Pol II
BRD4
PU.1
mediator
Pol II
Promoter
gene
Primed chromatin landscape
LPS stimuli
Enhancer
Pol II
NF-κB
BRD4
PU.1
NF-κB
Pol II
Promoter
gene
IL-6
IL-10
Robust and quick gene expression

Figure 5

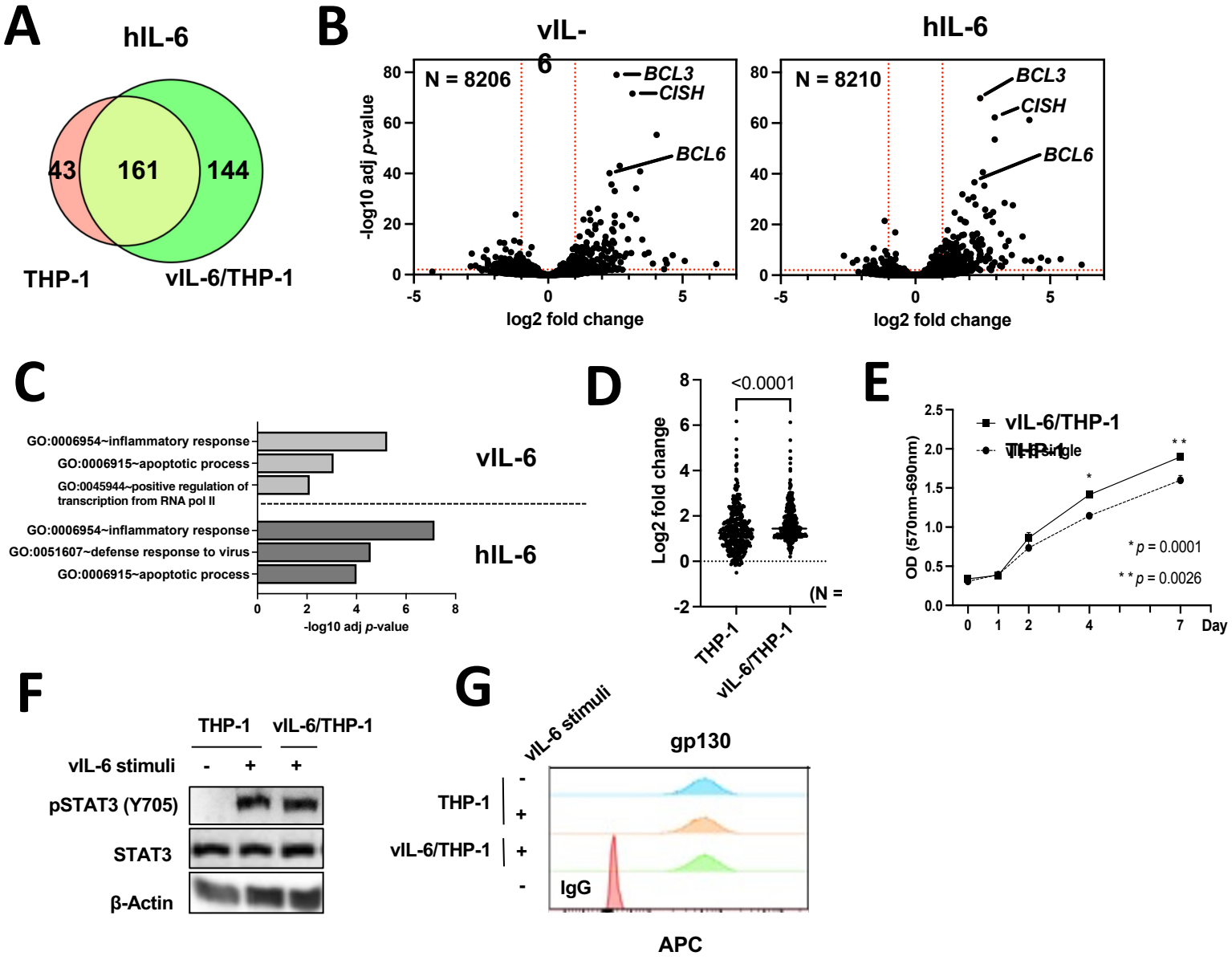

SFig.1 hIL-6 is a functional homolog of vIL-6 (A) The number of up-regulated genes (log2 fold change >1, adj *p*-value < 0.01) after hIL-6 stimulation. Red circle represents THP-1 cells and green circle represents vIL-6/THP-1 cells. **(B)** Individual gene expression in THP-1 cells with vIL-6 stimulation (left, N = 8206) and hIL-6 stimulation (right, N = 8210). Representative gene names were labelled adjacent to dots. The red dashed line indicated log2 fold change = ±1 (vertical) and -log10 adj p-value = 2 (horizontal). **(C)** KEGG pathway analysis performed on up-regulated genes (log2 fold change >1, adj *p*-value < 0.01) in THP-1 cells with vIL-6 and hIL-6 stimulation. The result showed the top three pathways each. **(D)** Individual up-regulated gene expression (N = 348) in parent THP-1 and vIL-6/THP-1 cells after hIL-6 stimulation. Data were analyzed using Wilcoxon matched-pairs signed ranked test and shown as median. **(E)** Measurement of cell proliferation with MTT assays. 1 X 10^4 THP-1 or vIL-6/THP-1 cells were cultured in triplicate in a 96 well plate. vIL-6 was added to vIL-6/THP-1 cells every other day. OD (570-690nm) was measured on day 0,1,2,4 and 7. Data were analyzed using unpaired Student's *t* test and shown as mean ± SD. **(F)** Immunoblotting with antibodies directed against STAT3, pshopho-STAT3 (Y705) and β-Actin (loading control) protein in THP-1 and vIL6/THP-1 cells. (G) FACS analysis showing the gp130 expression on cell surface.

SFig.1

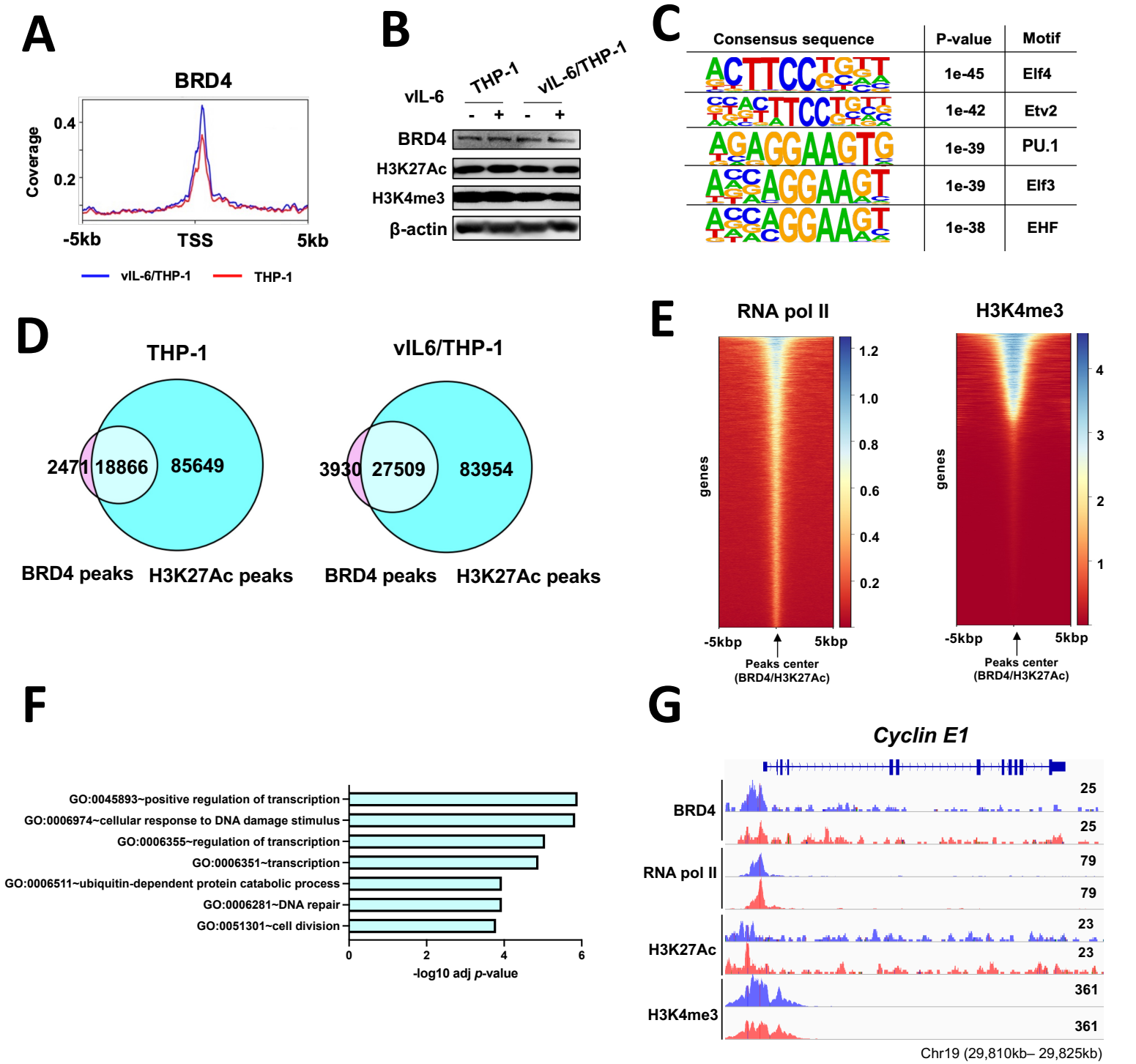

SFig.2 Prolonged vIL-6 exposure enhances the association of BRD4 and H3K27Ac **(A)** BRD4 CUT &RUN signals in ±5kbp windows around the transcription start sites (TSS) of up-regulated genes in vIL-6/THP-1 cells (N = 303). **(B)** BRD4, H3K27Ac and H3K4me3 protein expression before and after vIL-6 stimulation in parental THP-1 and vIL-6/THP-1 cells. **(C)** DNA binding motif analysis of new BRD4 accumulation sites in vIL-6/THP-1 cells. Images were drawn by findMotif (HOMER). **(D)** The number of BRD4 and H3K27Ac peaks and their association in parental THP-1 and vIL-6/THP-1 cells. The overlapping peaks were extracted using mergepeaks (HOMER). **(E)** RNA pol II and H3K4me3 CUT &RUN signals in ±5kbp windows around the center of BRD4 and H3K27Ac peaks. **(F)** KEGG pathway analysis performed on genes at BRD4 and H3K27 overlapping peaks in promoter regions in vIL-6/THP-1 cells. Results are presented in descending order. **(G)** BRD4, RNA pol II, H3K27Ac and H3K4me3 enrichment in the *Cyclin E1* promoter region in parental THP-1 cells (pink) and vIL-6/THP-1 cells (blue). The peaks were visualized by importing the BAM files into the Integrative Genomics Viewer (IGV).

SFig.2

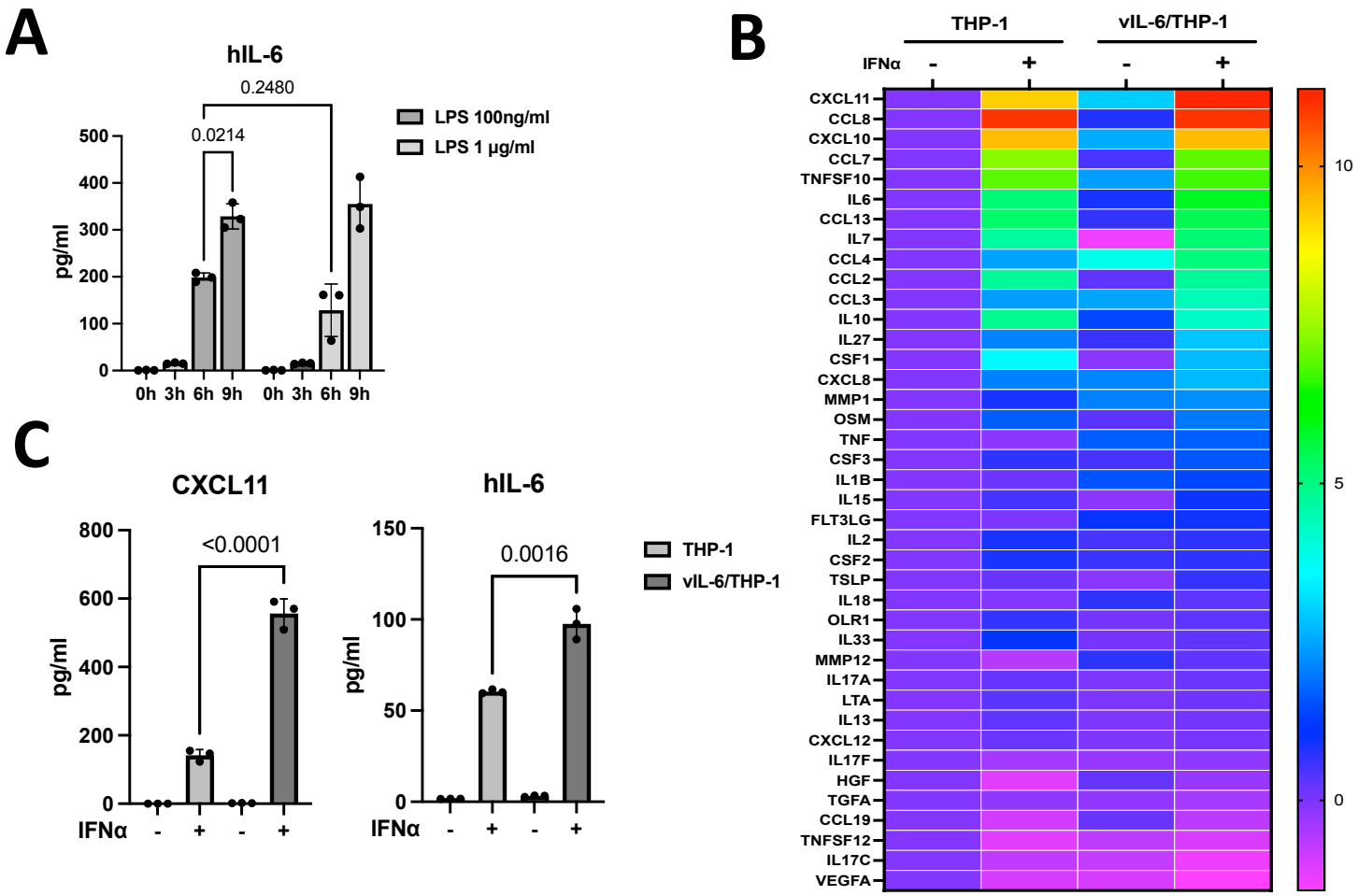

SFig.3 Inflammatory response to IFNα after vIL-6 prolonged exposure (A) hIL-6 production in THP-1 cells by LPS stimulation. THP-1 cells was incubated with LPS 100ng/ml or 1μg/ml for various time periods. Supernatants were harvested and incubated in triplicate in ELISA plate coated with hIL-6 antibody, Human IL-6 Uncoated ELISA kit (Invitrogen) was then used to evaluate the hIL-6 production by following the manufacturer's guideline. The protein binding measured as OD values at 450nm was shown. Results are presented as mean percentage viability ±SD ($n = 3$ samples/group). Data was analyzed by a one-way ANOVA test. **(B)** Heatmap showing the results of Olink® Target 48 Cytokine panel . IFNα (100ng/ml) was added to parent THP-1 cells or vil-6/THP-1 cells for 6 hours. Cytokine production in untreated THP-1 cells was set as 1 and $\log_2$ fold activation relative to untreated cells are shown. Samples were prepared in triplicate and the mean value were shown. **(C)** Inflammatory cytokine production determined by Olink proximity extension assay. Data was analyzed using two-sided unpaired Student's *t* test and shown as mean ± SD.

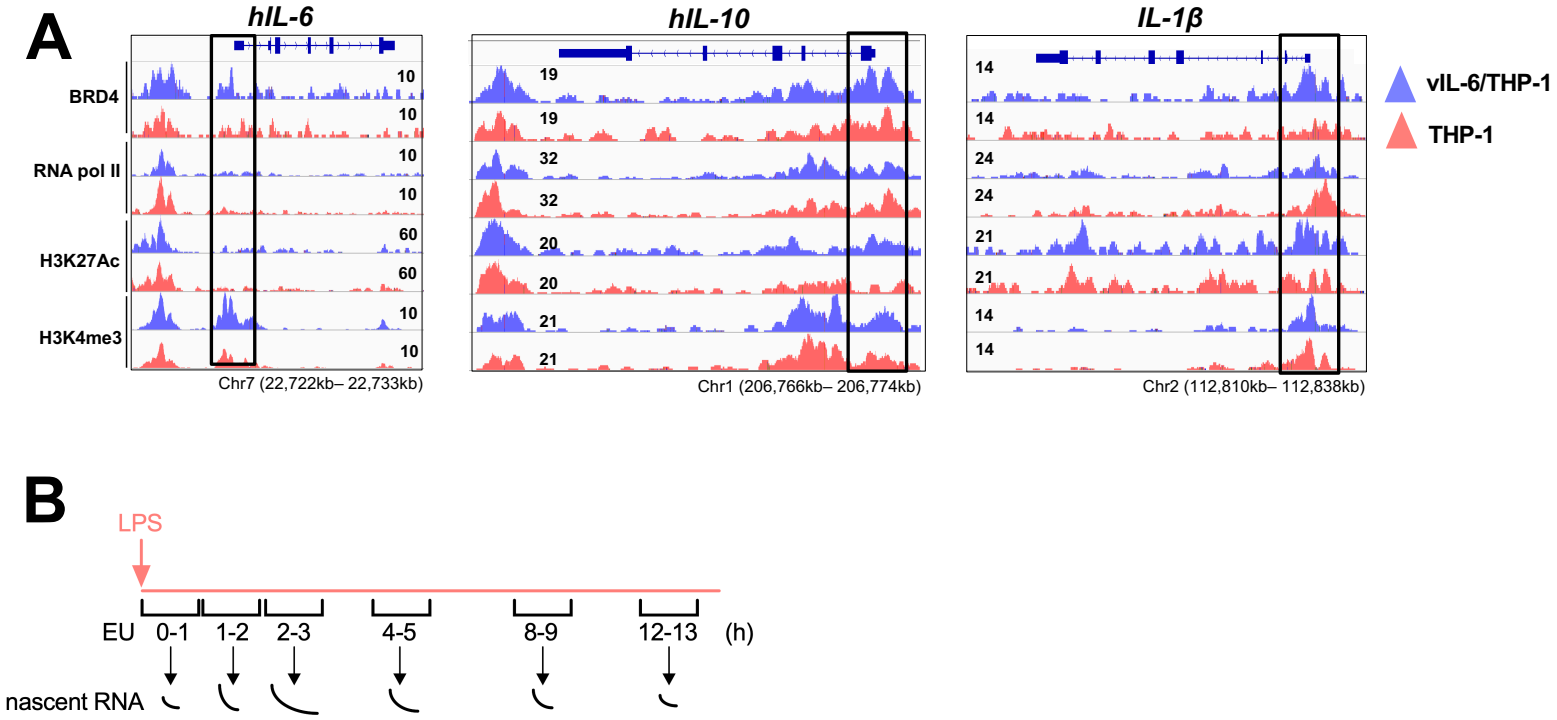

SFig.4 BRD4 enrichment in the promoter region of inflammatory genes (A) BRD4, RNA pol II, H3K27Ac and H3K4me3 enrichment in hIL-6, IL-10, IL-1β promoter region in parental THP-1 cells (pink) and vIL-6/THP-1 cells (blue). The promoter region is enclosed by a black line. Each CUT&RUN peak was visualized by importing the BAM files into Integrative Genomics Viewer (IGV). **(B)** Schematic diagram of nascent RNA labeling after LPS stimulation. LPS were added to culture medium in parental THP-1 and vIL-6/THP-1 cells and cells were incubated with EU for 1 hour in 0, 1, 2, 4 8, 12 h LPS stimulation.

Table. S1. Primer used for RT-qPCR and Chip-qPCR

RT-qPCR primer		
hIL-6	Forward	GGTACATCCTCGACGGCATCT
	Reverse	GTGCCTCTTTGCTGCTTT
IL-10	Forward	GGTTGCCAAGCCTTGTCTGA
	Reverse	AGGGAGTTCACATGCGCCT
IL-1β	Forward	AAACAGATGAAGTGCTCCTTCCAGG
	Reverse	TGGAGAACACCACTTGTTGCTCCA
18S rRNA	Forward	TTCGAACGTCTGCCCTATCAA
	Reverse	ATGGTAGGCACGGCGACTA
Chip-qPCR primer		
hIL-6 promoter	Forward	AACTTGGTTCAGGAGTGTCTAC
	Reverse	AGGATGGCTGGATGGTTTC
IL-10 promoter	Forward	GGAGATCTCGAAGCATGTTAGG
	Reverse	GGACAGAGAGGTGAAGGTCTA
IL-1β promoter	Forward	CAGCCAATCTTCATTGCTCAAG
	Reverse	CATACACACAAAGAGGCAGAGA